

3.3 Strongly Correlated Quantum Systems

Mechanism of quantum spin liquid and high- T_c superconductivity studied by excitation spectra and nonequilibrium dynamics calculation by variational Monte Carlo methods

Masatoshi IMADA

Toyota Physical and Chemical Research Institute

41-1 Yokomichi, Nagakute, Aichi, 480-1192

and

Research Institute for Science and Engineering, Waseda University

3-4-1 Okubo, Shinjuku-ku, Tokyo, 169-8555

Understanding physics of high- T_c cuprate superconductors remains one of the important problems in materials science. In this project, we have reproduced the experimental phase diagram of $\text{HgBa}_2\text{CuO}_{4+y}$ [1] by solving its *ab initio* low-energy effective Hamiltonian without adjustable parameters [2]. It shows a superconducting phase in a wide range of hole density δ , and its competition with charge period-4 plus spin period-8 stripe order near $\delta \sim 0.1$, in agreement with experimental results.

A crucial role of off-site interactions in stabilizing the superconductivity is elucidated with emphasis on charge fluctuations. It also clarifies the condensation energy mainly contributed from the on-site Coulomb interaction. The present achievement will enable deeper, predictable understanding on open issues of the high- T_c superconducting mechanism and promote *ab initio* studies on strongly correlated electrons beyond parametrized model studies.

In former studies on a simplified effective

model, namely Hubbard model on the square lattice had clarified that the *d*-wave superconducting state is severely competing with the stripe ordered state, while most of the phase diagram in the parameter space of the carrier doping concentration is dominated by the stripe order and the superconducting state remains an excited state [3,4]. Therefore, the Hubbard model does not properly account for the experimental phase diagram of the cuprate superconductors. However, it has also been shown that the superconducting phase in the *ab initio* Hamiltonian is adiabatically connected with that found in the superconducting excited state of the Hubbard model. Therefore, it is intriguing to understand the distinction of the superconducting state in between the *ab initio* and Hubbard cases. The method for dynamical properties newly developed offer useful insights into this issue as we describe in the next section.

Calculations of dynamical quantities are a challenging subject for strongly correlated electron systems even in the linear response

regime. Recently we have developed a method to calculate the dynamical correlation functions based on the variational Monte Carlo method [3,4]. We first developed a method to calculate the charge dynamical structure factors for the ground states of correlated electron systems. Our benchmarks for the one- and two-dimensional Hubbard models show that inclusion of composite-fermion excitations in the basis set greatly improves the accuracy, in reference to the exact charge dynamical structure factors for clusters. Together with examination for larger systems beyond tractable sizes by the exact diagonalization, our results indicate that the variational Monte Carlo method is a promising way for studies on the nature of charge dynamics in correlated materials such as the copper oxide superconductors if the composite-fermion excitations are properly included in the restricted Hilbert space of intermediate states in the linear response theory. Our results on the charge dynamical structure factor are consistent with the particle-hole excitations inferred from the single-particle spectral function $A(k,\omega)$ in the literature. The importance of incorporating nonlocal composite fermion for a more accurate description is also pointed out [3].

This method can be extended to calculate the one-body Green's function by improving the variational Monte Carlo method. We benchmark against the exact diagonalization for the one- and two-dimensional Hubbard models of 16 site lattices, which proves high accuracy of the

method. The application of the method to larger-sized Hubbard model on the square lattice correctly reproduces the Mott insulating behavior at half filling and gap structures of d -wave superconducting state of the hole doped Hubbard model in the ground state optimized by enforcing the charge uniformity, evidencing a wide applicability to strongly correlated electron systems.

From the obtained d -wave superconducting gap of the charge uniform state, we find that the gap amplitude at the antinodal point is several times larger than the experimental value, when we employ a realistic parameter as a model of the cuprate superconductors. The effective attractive interaction of carriers in the d -wave superconducting state inferred for an optimized state of the Hubbard model is as large as the order of the nearest-neighbor transfer, which is far beyond the former expectation in the cuprates. The nature of the superconducting state of the Hubbard model in terms of the overestimate of the gap and the attractive interaction in comparison to the cuprates are clarified [4].

Finding quantum spin liquids is another important subject of the present research project. Topological properties of the strongly correlated systems with strong spin-orbit interaction are one of such subjects. We have studied Heisenberg model with spin-orbit interaction (Dzyaloshinskii-Moriya interaction) on the pyrochlore lattice by using the variational Monte

Carlo method. This system has been proposed to be a candidate of the quantum spin liquid in earlier studies. We will report the result on this subject in the future.

Another candidate of the quantum spin liquid is found in a quantum Heisenberg model with the geometrically frustrated square lattice, called J_1 - J_2 model. By utilizing the machine learning method, we have found a firm evidence for the quantum spin liquid and clarified its excitation spectra, which indicate the fractionalization of spins into spinons. The subject has a close connection to the experimentally observed spin liquid state in molecular conductors. Studies on the *ab initio* low-energy effective Hamiltonian for a dmit compound are underway and will be reported elsewhere.

This is a combined report for E project “Mechanism of quantum spin liquid and high- T_c superconductivity studied by excitation spectra and nonequilibrium dynamics calculation by variational Monte Carlo methods”, “Development of methodology for analysis of nonequilibrium superconductivity in strongly correlated systems via integration of electronic state theory and time-resolved experimental data”, and shared project for post-K project “Studies on quantum spin liquids in molecular

conductors based on first-principles Hamiltonian”.

and “Studies on Quantum Spin Liquids in Materials with Strong Spin-Orbit Interaction”

This series of work has been done in collaboration with T. Ohgoe, T. Misawa, M. Hirayama, K. Ido, Y. Nomura, Y. Yamaji, R. Pohle and M. Charlebois. The calculations were performed on computers at the Supercomputer Center, ISSP, Univ. of Tokyo. The work is also supported by JSPS Kakenhi 16H06345, the RIKEN Center for Computational Science under the HPCI project (hp190145) and the MEXT HPCI Strategic Programs, CDMSI. This project has used the software HPhi and mVMC.

References

- [1] Motoaki Hirayama, Takahiro Misawa, Takahiro Ohgoe, Youhei Yamaji, Masatoshi Imada, Phys. Rev. B **99** (2019) 245155.
- [2] Takahiro Ohgoe, Motoaki Hirayama, Takahiro Misawa, Kota Ido, Youhei Yamaji, Masatoshi Imada, Phys. Rev. B **101** (2020) 045124.
- [3] Kota Ido, Masatoshi Imada, Takahiro Misawa, Phys. Rev. B **101** (2020) 075124.
- [4] Maxime Charlebois, and Masatoshi Imada, arXiv:1912.09960.

Numerical studies on energy current correlations in frustrated quantum spin systems

Youhei YAMAJI

*Department of Applied Physics, The University of Tokyo
Hongo 7-3-1, Bunkyo-ku, Tokyo 113-8656*

Topological states of matters are often characterized by quantized transport properties. As a prototypical example, two dimensional Chern insulators are characterized by the quantized charge Hall effect. In the Mott insulators, however, the quantization of thermal Hall transports characterizes the topological states, instead of the charge transports [1, 2]. The quantum spin liquid state of the Kitaev model is a typical example of the topological state that shows half-integer quantized thermal Hall transports [1]. The observation of the half-integer quantized thermal Hall coefficient in a spin-orbit coupled Mott insulator α -RuCl₃ has attracted broad attention [3].

We studied numerical methods to characterize the topological spin liquids. The thermal transport is calculated by correlations of thermal currents and energy magnetization [4]. These quantities are formulated by energy current operators, which are given by the continuity equation of the energy density.

For the lattice hamiltonian, the energy density is represented by the bond energy as follows. Here, we show the continuity equation of the energy density of the Kitaev-type magnets on the honeycomb lattice as an example. The nearest-neighbor bonds on the honeycomb lattice have three different directions. When the three bonds are labeled as x , y , and z , an effective hamiltonian of α -RuCl₃, the Kitaev- Γ

hamiltonian,

$$\hat{H} = \sum_{\gamma=x,y,z} \sum_{\langle \ell,m \rangle \in \gamma} \hat{H}_{\ell m}^{(\gamma)}, \quad (1)$$

is defined by the exchange coupling for the γ ($= x, y, z$) bond,

$$\hat{H}_{\ell m}^{(\gamma)} = K \hat{S}_{\ell}^{\gamma} \hat{S}_{m}^{\gamma} + \Gamma \left(\hat{S}_{\ell}^{\alpha} \hat{S}_{m}^{\beta} + \hat{S}_{\ell}^{\beta} \hat{S}_{m}^{\alpha} \right) \quad (2)$$

where (α, β, γ) is a permutation of (x, y, z) and K (Γ) is the Kitaev (off-diagonal symmetric) exchange coupling. The bond energy of the hamiltonian is, then, introduced as the Fourier components,

$$\begin{aligned} \hat{H}_{\mathbf{q}} &= \sum_{\gamma} \sum_{\langle \ell,m \rangle_{\gamma}} e^{+i(\mathbf{q}/2) \cdot (\mathbf{R}_{\ell} + \mathbf{R}_m)} \\ &\times \left[K \hat{S}_{\ell}^{\gamma} \hat{S}_{m}^{\gamma} + \Gamma \left(\hat{S}_{\ell}^{\alpha} \hat{S}_{m}^{\beta} + \hat{S}_{\ell}^{\beta} \hat{S}_{m}^{\alpha} \right) \right], \quad (3) \end{aligned}$$

where $\epsilon_{\alpha\beta\gamma}$ ($\alpha, \beta, \gamma = x, y, z$). By using the small \mathbf{q} limit of the continuity equation of the bond energy,

$$\frac{d\hat{H}_{\mathbf{q}}}{dt} \sim -i\mathbf{q} \cdot \mathbf{j}_E, \quad (4)$$

we determine the energy current operator \mathbf{j}_E . When, for simplicity, $K = 0$ is chosen, the Heisenberg equation of motion,

$$\frac{d\hat{H}_{\mathbf{q}}}{dt} = \frac{i}{\hbar} \left[\hat{H}, \hat{H}_{\mathbf{q}} \right], \quad (5)$$

defines \mathbf{j}_E with the commutator,

$$\begin{aligned}
\frac{i}{\hbar} [\hat{H}, \hat{H}\mathbf{q}] &= \frac{i}{\hbar} \Gamma^2 \sum_{\ell} \left[\mathbf{q} \cdot \boldsymbol{\delta}_{xz,\ell} \left(\hat{S}_{m_x}^y \hat{S}_{\ell}^x \hat{S}_{m_z}^x + \hat{S}_{m_x}^z \hat{S}_{\ell}^z \hat{S}_{m_z}^y - \hat{S}_{m_x}^y \hat{S}_{\ell}^y \hat{S}_{m_z}^y \right) \right. \\
&\quad + \mathbf{q} \cdot \boldsymbol{\delta}_{zy,\ell} \left(\hat{S}_{m_z}^x \hat{S}_{\ell}^z \hat{S}_{m_y}^z + \hat{S}_{m_z}^y \hat{S}_{\ell}^y \hat{S}_{m_y}^x - \hat{S}_{m_z}^x \hat{S}_{\ell}^x \hat{S}_{m_y}^y \right) \\
&\quad \left. + \mathbf{q} \cdot \boldsymbol{\delta}_{yx,\ell} \left(\hat{S}_{m_y}^z \hat{S}_{\ell}^y \hat{S}_{m_x}^y + \hat{S}_{m_y}^x \hat{S}_{\ell}^x \hat{S}_{m_x}^z - \hat{S}_{m_y}^z \hat{S}_{\ell}^z \hat{S}_{m_x}^x \right) \right] \\
&\quad + \frac{i}{\hbar} \Gamma^2 \sum_m \left[\mathbf{q} \cdot \boldsymbol{\delta}_{xz,m} \left(\hat{S}_{\ell_x}^y \hat{S}_m^x \hat{S}_{\ell_z}^x + \hat{S}_{\ell_x}^z \hat{S}_m^z \hat{S}_{\ell_z}^y - \hat{S}_{\ell_x}^y \hat{S}_m^y \hat{S}_{\ell_z}^z \right) \right. \\
&\quad + \mathbf{q} \cdot \boldsymbol{\delta}_{zy,m} \left(\hat{S}_{\ell_z}^x \hat{S}_m^z \hat{S}_{\ell_y}^z + \hat{S}_{\ell_z}^y \hat{S}_m^y \hat{S}_{\ell_y}^x - \hat{S}_{\ell_z}^x \hat{S}_m^x \hat{S}_{\ell_y}^y \right) \\
&\quad \left. + \mathbf{q} \cdot \boldsymbol{\delta}_{yx,m} \left(\hat{S}_{\ell_y}^z \hat{S}_m^y \hat{S}_{\ell_x}^y + \hat{S}_{\ell_y}^x \hat{S}_m^x \hat{S}_{\ell_x}^z - \hat{S}_{\ell_y}^z \hat{S}_m^z \hat{S}_{\ell_x}^x \right) \right], \tag{6}
\end{aligned}$$

where $\boldsymbol{\delta}_{\alpha\beta,\ell}$ is the vector from the center of the α -bond terminated by ℓ th site and to the center of the β -bond terminated also by ℓ th site.

The energy-current–energy-current correlations and energy magnetization for the Kitaev- Γ hamiltonian at finite temperatures are calculated by combining the Krylov subspace methods and typicality approaches [5] and will be reported elsewhere [6].

The topological nature of the Mott insulating states will be destroyed by spontaneous symmetry breakings. Therefore, to clarify the topology, we need to examine whether the spin liquid candidates show spontaneous symmetry breakings or not. We have modified mVMC [7] to calculate higher-order spin correlations and calculated the singlet-singlet correlators of a typical frustrated quantum spin systems, the Heisenberg model on pyrochlore lattices. So far, the inversion symmetry is spontaneously broken in the lowest variational state.

References

- [1] A. Kitaev: Ann. Phys. **321** (2006) 2.
- [2] C. Wang, A. C. Potter, and T. Senthil: Science **343** (2014) 6171.
- [3] Y. Kasahara, *et al.*: Nature **559** (2018) 227.
- [4] T. Qin, Q. Niu, and J. Shi: Phys. Rev. Lett. **107** (2011) 236601.
- [5] Y. Yamaji, T. Suzuki, and M. Kawamura: arXiv:1802.02854.
- [6] Y. Yamaji, *et al.*: in preparation.
- [7] T. Misawa, *et al.*: Compt. Phys. Commun. **235** (2019) 447.

Theoretical study of spin-orbit coupled phenomena in correlated electron systems

Yukitoshi MOTOME

Department of Applied Physics,

The University of Tokyo, Bunkyo, Tokyo 113-8656

We have theoretically studied a variety of intriguing phenomena in correlated electron systems with spin-orbit coupling, ranging from Mott insulators to metals. During this fiscal year, we have achieved substantial progress on the following topics (project numbers: H31-Ca-0052 and H31-Cb-0032). We summarize the main results below.

(i) *Kitaev quantum spin liquids*: By using *ab initio* based calculations, we theoretically proposed new candidates for the Kitaev magnets with unconventional antiferromagnetic Kitaev interactions: Pr-based *f*-electron compounds [1,2] and polar asymmetric systems [3]. We also clarified real-time dynamics of fractional excitations in the Kitaev quantum spin liquids [4], Majorana-magnon crossover in an applied magnetic field [5], and exotic phase transitions in three-dimensional extensions of the Kitaev models [6,7]. In addition, we have collaborated with several experimental groups for identifying the signatures of Majorana excitations in the Kitaev magnets: nuclear quadrupole and magnetic resonances [8], Raman scattering [9], and thermal Hall effect [10]. We have summarized the recent results on

this topic in review articles [11,12,13].

(ii) *Chiral magnets*: We theoretically unveiled that a nonreciprocal spin transport, which is switchable by a magnetic field, can occur in monoaxial magnets [14]. We also clarified that interplay between spin, charge, and orbital degrees of freedom plays a crucial role in stabilizing the magnetic hedgehog lattices recently found in *B20* chiral magnets [15]. We also showed that the magnetic monopoles and antimonopoles associated with the magnetic hedgehogs annihilate in pair by magnetic fields and cause topological phase transitions [15,16].

(iii) *Multipole physics*: We theoretically proposed that the successive phase transitions in a spin-orbit coupled metal $\text{Cd}_2\text{Re}_2\text{O}_7$ are driven by electric toroidal quadrupoles [17]. We also clarified that nonmagnetic impurities can induce magnetic and toroidal multipoles in ferromagnets [18].

(iv) *Spin current generation*: We discovered a new mechanism of spin current generation, which can work even in the absence of the spin-orbit coupling [19]. We also developed the understanding of this phenomenon based on the cluster multipole picture [20].

References

- [1] S.-H. Jang, R. Sano, Y. Kato, and Y. Motome, Phys. Rev. B **99**, 241106(R) (2019).
- [2] S.-H. Jang, R. Sano, Y. Kato, and Y. Motome, preprint (arXiv:1912.03422).
- [3] Y. Sugita, Y. Kato, and Y. Motome, Phys. Rev. B **101**, 100410(R) (2020).
- [4] J. Nasu and Y. Motome, Phys. Rev. Research **1**, 033007 (2019).
- [5] J. Yoshitake, J. Nasu, Y. Kato, and Y. Motome, Phys. Rev. B **101**, 100408(R) (2020).
- [6] T. Eschmann, P. A. Mishchenko, T. A. Bojesen, Y. Kato, M. Hermanns, Y. Motome, and S. Trebst, Phys. Rev. Research **1**, 032011(R) (2019).
- [7] P. A. Mishchenko, Y. Kato, K. O'Brien, T. A. Bojesen, T. Eschmann, M. Hermanns, S. Trebst, and Y. Motome, Phys. Rev. B **101**, 045118 (2020), *Editors' Suggestion*.
- [8] Y. Nagai, T. Jinno, Y. Yoshitake, J. Nasu, Y. Motome, M. Itoh, and Y. Shimizu, Phys. Rev. B **101**, 020414(R) (2020).
- [9] Y. Wang, G. B. Osterhoudt, Y. Tian, P. Lampen-Kelley, A. Banerjee, T. Goldstein, J. Yan, J. Knolle, H. Ji, J. Cava, J. Nasu, Y. Motome, S. Nagler, D. Mandrus, and K. S. Burch, npj Quant. Mat. **5**, 14 (2020).
- [10] T. Yokoi, S. Ma, Y. Kasahara, S. Kasahara, T. Shibauchi, N. Kurita, H. Tanaka, J. Nasu, Y. Motome, C. Hickey, S. Trebst, and Y. Matsuda, preprint (arXiv:2001.01899).
- [11] Y. Motome and J. Nasu, J. Phys. Soc. Jpn. **89**, 012002 (2020), *INVITED REVIEW PAPER*.
- [12] 求 幸年, 那須 讓治, 固体物理 **54**, 217 (2019).
- [13] Y. Motome, R. Sano, S.-H. Jang, Y. Sugita, and Y. Kato, preprint (arXiv:2001.03731), in press in J. Phys.: Condens. Matter, *Special Issue Article*.
- [14] S. Okumura, H. Ishizuka, Y. Kato, J. Ohe, and Y. Motome, Appl. Phys. Lett. **115**, 012401 (2019).
- [15] S. Okumura, S. Hayami, Y. Kato, and Y. Motome, preprint (arXiv:1908.05044), in press in Phys. Rev. B.
- [16] S. Okumura, S. Hayami, Y. Kato, and Y. Motome, JPS Conf. Proc. **30**, 011010 (2020).
- [17] S. Hayami, Y. Yanagi, H. Kusunose, and Y. Motome, Phys. Rev. Lett. **122**, 147602 (2019), *selected as a Cover Image*.
- [18] S. Hayami, H. Kusunose, and Y. Motome, J. Phys. Soc. Jpn. **88**, 063702 (2019).
- [19] M. Naka, S. Hayami, H. Kusunose, Y. Yanagi, Y. Motome, and H. Seo, Nat. Commun. **10**, 4305 (2019).
- [20] S. Hayami, Y. Yanagi, M. Naka, H. Seo, Y. Motome, and H. Kusunose, JPS Conf. Proc. **30**, 011149 (2020).

Numerical Studies on the Role of the Incipient Band Played in Two-band Unconventional Superconductivity

KAZUHIKO KUROKI

Department of Physics, Osaka University

1-1 Machikaneyama, Toyonaka, Osaka, 560-0043, Japan

We have been studying spin-fluctuation-mediated superconductivity in two-band systems with one of the bands intersecting the Fermi level while the other band (“incipient band”) sits in the vicinity of the Fermi level. In ref.[1, 2], we studied the Hubbard model on a two-leg ladder lattice, which is characterized by the nearest neighbor hoppings in the leg (t) and the rung (t_r) directions, and also the diagonal next nearest neighbor hoppings t' (Fig.1).

In 2019 fiscal year, we have extended the study to two dimensional (2D) systems. A simplest extension of the two-leg ladder Hubbard model to two dimensions is the bilayer square lattice Hubbard model, where two Hubbard models on a square lattice are coupled by vertical hoppings t_\perp along with diagonal hoppings t' (Fig.1). Here, t_\perp controls the relative energy between the two bands like t_r in the two-leg ladder. We adopted the fluctuation exchange (FLEX) approximation, and solved the linearized Eliashberg equation to obtain the eigenvalue at a fixed temperature ($T = 0.05t$), which gives a measure for the superconducting transition temperature. We investigated a large parameter space of (t_\perp, t', n, U) , where n is the band filling and U is the on-site Hubbard interaction.[3] Simultaneously, we also performed similar calculation for

the two-leg ladder Hubbard model, and made a comparison between the two models.

In Fig.2, we show for $t' = 0$ the eigenvalue λ plotted against t_\perp for the bilayer and t_r for the two-leg ladder. For each t_\perp or t_r , the maximum eigenvalue is searched by varying the band filling n . We perform the calculation for $U = 6t$ and $U = 3t$. For $U = 6t$ in the bilayer and for both values of U in the ladder, λ is maximized when the bonding band touches the Fermi level, i.e., when the band is incipient. This is not the case for $U = 3t$ in the

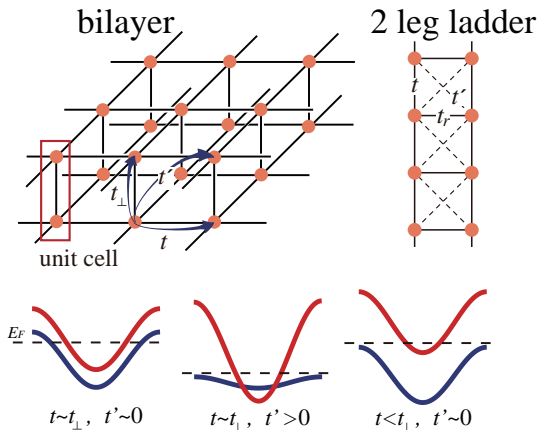


FIG. 1. Upper panel : the bilayer lattice (left) and the two-leg ladder lattice (right). Lower panels : schematic images of the bonding and antibonding bands of the bilayer lattice. Left : $t \sim t_\perp$, $t' \sim 0$, middle : $t \sim t_\perp$, $t' > 0$, right : $t < t_\perp$, $t' \sim 0$. In the middle and right panels, the bonding band is incipient.

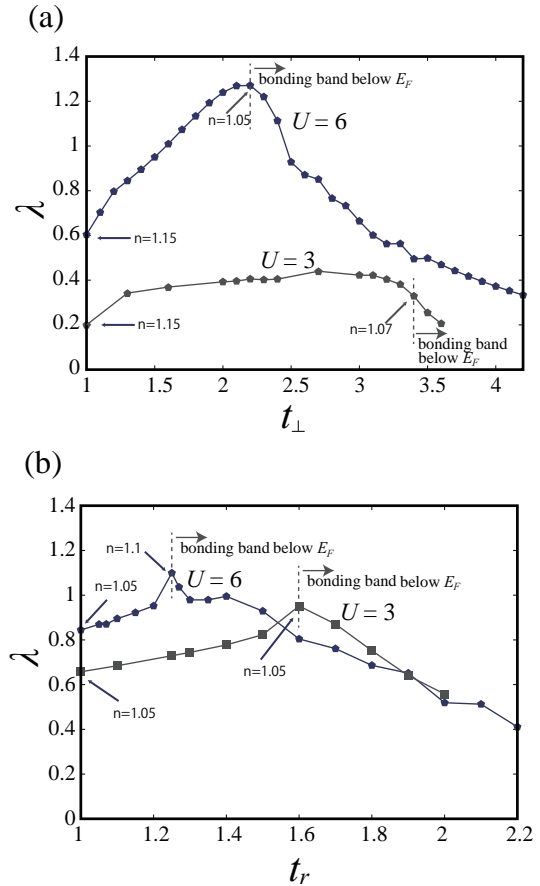


FIG. 2. (a) Maximized λ at $T = 0.05$ of the bilayer Hubbard model with $U = 6t$ or $3t$ and $t' = 0$ plotted against t_\perp . λ is maximized at each t_\perp by varying the band filling n . At some points, n that maximizes λ is denoted by arrows. (b) Similar plot for the two-leg Hubbard ladder model, where t_\perp is replaced by t_r . From Ref.[3].

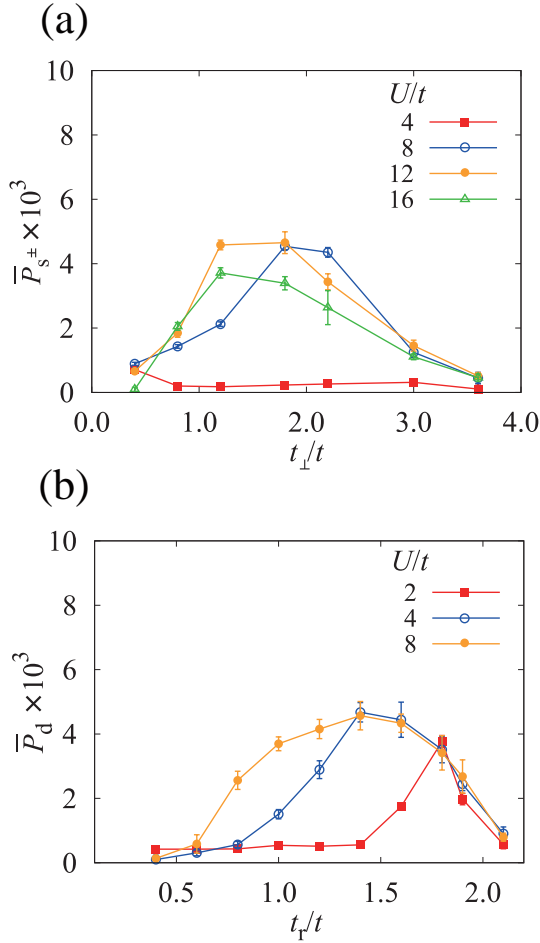


FIG. 3. mVMC calculation results of the pairing correlation for the two models with $t' = 0$. (a) t_{\perp}/t dependence of the pairing correlation $\bar{P}_{s\pm}$ (interlayer nearest neighbor pairing) for the bilayer model with various values of U/t . The band filling is $n = 1.06$. (b) t_r dependence of the pairing correlation \bar{P}_d (interchain nearest neighbor pairing) for the two-leg ladder model with various values of U/t . The band filling is $n = 1.03$. From Ref.[6].

bilayer, where λ is significantly reduced.

We also performed multivariable variational Monte Carlo calculation (mVMC) [4, 5] study for the two models, and calculated the pairing correlation function against t_{\perp} (bilayer) or t_r (two-leg ladder)[6]. The results shown in Fig.3 resemble the FLEX results of the eigenvalue of the Eliashberg equation shown in Fig.2 (note that FLEX is performed only in the $t_{\perp} \geq t$ or $t_r \geq t$ regime).

The above FLEX and mVMC results suggest that, when U is sufficiently large, superconductivity is strongly enhanced in both the bilayer and two-leg ladder models when the bonding band is incipient. As t_{\perp} or t_r becomes small and the bonding band intersects the Fermi level, superconductivity is significantly degraded for the bilayer model, but not so strongly in the ladder. When U be-

comes small, the overall tendency does not change much in the ladder (except that larger t_r is needed for the bonding band to be incipient because the band width renormalization is weak), but for the bilayer model, superconductivity is strongly suppressed and it is no longer optimized in the incipient band situation.

It is known that the spin fluctuations within a certain moderate energy range work effectively as pairing glue, while those in the very low energy range are pair breaking[7]. This, combined with the difference in the density of states (DOS) for the two models due to the difference in the dimensionality, enables us to understand the obtained results[3, 6]. Namely, when the bonding band is incipient, the low-energy spin fluctuations is suppressed because only the states around the bonding band edge can contribute to their development, while there is significant contribution from the bonding band to the moderate-energy spin-fluctuations. This is the reason why superconductivity is strongly enhanced in the incipient band situation. As t_{\perp} or t_r is reduced and the bonding band intersects the Fermi level, the low energy spin fluctuation rapidly develops in the bilayer lattice because the DOS of the bonding band at the Fermi level increases, while the development of the low energy spin fluctuation in the ladder is moderate because the DOS of the bonding band decreases as the Fermi level moves toward the middle of the band. This explains the difference between the two models. As for the effect of U , the band width is reduced by the renormalization, so that the bonding band becomes incipient for a smaller t_{\perp} or t_r for larger U . This effect is essential for superconductivity to be strongly enhanced in the bilayer model because in this way the portion of the DOS that contributes to superconductivity is squeezed into a narrower energy range. This effect is not so important in the ladder, where the DOS at the band edge is diverging.

-
- [1] K. Kuroki, T. Higashida, and R. Arita, Phys. Rev. B **72**, 212509 (2005).
 - [2] K. Matsumoto, D. Ogura, and K. Kuroki, Phys. Rev. B **97**, 014516 (2018).
 - [3] K. Matsumoto, D. Ogura, and K. Kuroki, J. Phys. Soc. Jpn. **89**, 044709 (2020).
 - [4] D. Tahara and M. Imada, J. Phys. Soc. Jpn. **77**, 114701 (2008).
 - [5] T. Misawa *et al.*, Comp. Phys. Comm. **235**, 447 (2019).
 - [6] D. Kato and K. Kuroki, Phys. Rev. Research, to appear (2020) (arXiv:1912.11983).
 - [7] A.J. Millis, S. Sachdev and C.M. Varma, Phys. Rev. B **37**, 4975 (1988).

Study of magnetism and transport phenomena in strongly correlated quantum systems using computational approaches including non-equilibrium methods

Norio KAWAKAMI

Department of Physics,

Kyoto University, Kitashirakawa, Sakyo-ku, Kyoto 606-8502

We have studied strongly correlated quantum systems with a focus on magnetism and transport phenomena, using computational approaches, including non-equilibrium methods.

We have analyzed the effect of correlations on the emergence of quantum oscillation in narrow-gap topological Kondo insulators by performing dynamical mean-field theory (DMFT) calculations. We have demonstrated that the interplay between correlations and nonlocal hybridizations can lead to observable quantum oscillations even without a Fermi surface and that quantum oscillations in a three-dimensional system can be understood from the physics of the two-dimensional planes in the momentum space for which the hybridization in the direction of the magnetic field vanishes. This scenario should be relevant for understanding the observations in SmB_6 and YbB_{12} . [1]

We have studied the impact of non-Hermiticity due to strong correlations in f -electron materials, by analyzing the periodic-Anderson model with local and nonlocal hybridization in the insulating and metallic regimes by DMFT combined with numerical renormalization group (NRG). We have shown that exceptional points, momenta in the

Brillouin zone at which the effective non-Hermitian Hamiltonian cannot be diagonalized, occur at the Kondo temperature, at which the magnetic moments are screened, and the well-known crossover between localized and itinerant f electrons takes place. [2]

Furthermore, we have studied the one-band Hubbard model on the honeycomb lattice by DMFT as well as by numerically exact quantum Monte Carlo simulations. We have shown that the DMFT approximation is very accurate in the Dirac semi-metallic phase, where local moment formation is present, and the spin correlation length small. Moreover, we have shown that although the quantum critical point can only be understood by lattice Quantum Monte Carlo techniques, DMFT gives a reasonable estimate of the critical interaction strength. [3]

References

- [1] R. Peters, T. Yoshida, and N. Kawakami, *Phys. Rev. B* **100**, 085124 (2019).
- [2] Y. Michishita, T. Yoshida, and R. Peters, *Phys. Rev. B* **101**, 085122 (2020).
- [3] M. Raczkowski, R. Peters, T. T. Phung, N. Takemori, F. F. Assaad, A. Honecker, and J. Vahedi, *Phys. Rev. B* **101**, 125103 (2020).

Study on metal-insulator transition in nickel oxides

Yusuke NOMURA

RIKEN Center for Emergent Matter Science, 2-1 Hirosawa, Wako, 351-0198

Rare-earth nickelates LuNiO_3 shows an interesting phase diagram. Starting from the room temperature, by cooling, it exhibits two-step transitions. The first one is the metal-insulator transition, and the second one is the magnetic transition. At the first transition, interestingly, bond disproportionation occurs, where one set of octahedra is compressed, and the other is expanded. It means that the displacement of breathing phonon mode is induced, and the Jahn-teller mode becomes inactive despite the $(e_g)^1$ configuration.

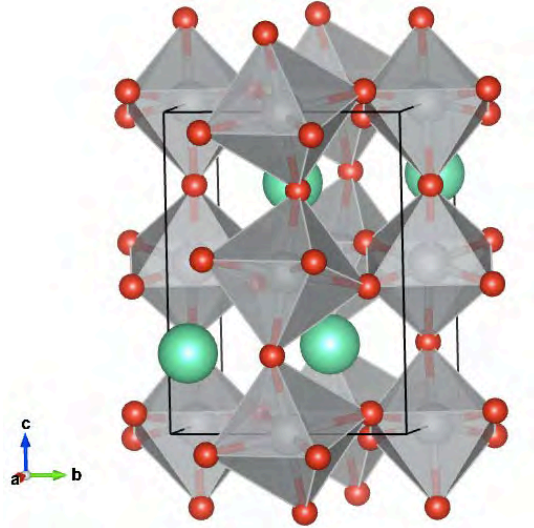


Fig. 1: Crystal structure of LuNiO_3 at high temperature.

In this study, we derive the effective low-

energy Hamiltonians for LuNiO_3 e_g manifold. We explicitly include the phonon degrees of freedom using newly-developed constrained density functional perturbation theory (cDFPT) [1]. We calculate the magnitude of phonon-mediated electron-electron interaction as well as the effective Coulomb interactions.

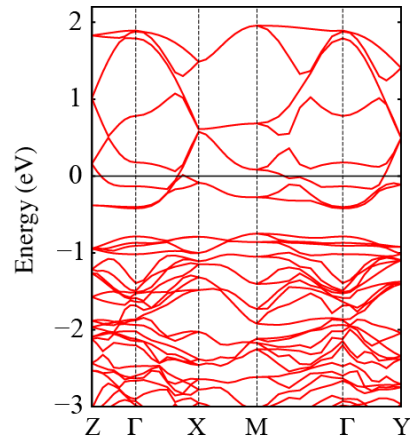


Fig. 2: Band structure of LuNiO_3 .

As a result, we find that coupling to the Jahn-Teller phonon mode indeed exists, which favors Jahn-Teller distortion. However, at the same time, non-local Coulomb interaction, which favors bond disproportionation, is substantial. Therefore, the coupling to Jahn-Teller mode and the non-local Coulomb interaction compete with each other. In the real material, the latter wins, and the bond disproportionation takes

place at the metal-insulator transition.

References

- [1] YN et al., Phys. Rev. Lett. **112**, 027002 (2014); YN and R. Arita, Phys. Rev. B **92**, 245108 (2015)

Study on frustrated magnetism using machine learning

Yusuke NOMURA

RIKEN Center for Emergent Matter Science, 2-1 Hirosawa, Wako, 351-0198

Quantum spin liquid (QSL) is an exotic state of the matter, in which long-range magnetic order is suppressed even at zero temperature. The QSL has attracted much attention not only because of its unique property such as the fractionalization of the excitation but also because of possible applications to quantum computing and memory devices. However, to show the existence of the QSL in the realistic quantum-spin Hamiltonians, except for rare cases such as the Kitaev model where the exact ground state can be constructed by hand, we need highly accurate numerical methods.

To achieve high accuracy, we focus on machine learning. Machine learning is good at extracting essential patterns in the data. By applying it to the quantum-many body problems, we can obtain an accurate representation of the quantum many-body wave functions (vector with exponentially large dimensions) with a finite number of parameters (data compression). Starting from the seminal work by Carleo and Troyer [1], now, there is growing evidence for the powerfulness of the machine learning method to study many-body problems. However, studies so far are limited to

the benchmark to check the usefulness of machine learning, and interesting applications to explore many-body physics have not yet performed.

In the study, by using a newly-developed machine learning method (RBM+PP), which combines the restricted Boltzmann machine (RBM) and pair-product (PP) state [2], we obtain strong support for the existence of the QSL phase in the thermodynamic limit of the spin-1/2 Heisenberg spin system on the square lattice with the nearest-neighbor and next-nearest-neighbor exchanges, J_1 and J_2 , respectively, called the J_1 - J_2 Heisenberg model. The QSL phase shows unconventional excitation spectrum, in which both the singlet and triplet excitations become gapless at high-symmetry momenta $(0,0)$, $(\pi,0)$, $(0,\pi)$, (π,π) , in support of the nodal Dirac dispersion of the fractionalized spinon at $(\pm\pi/2, \pm\pi/2)$.

References

- [1] G. Carleo and M. Troyer, *Science* **355**, 602 (2017).
- [2] Y. Nomura, A. S. Darmawan, Y. Yamaji, and M. Imada, *Phys. Rev. B* **96**, 205152 (2017).

Variational Monte Carlo calculation of two-dimensional Wigner crystal under lattice commensurability

Takeo KATO

*Institute for Solid State Physics, University of Tokyo
Kashiwa-no-ha, Kashiwa, Chiba 277-8581*

Wigner crystallization, which breaks the translational symmetry due to the long-range Coulomb interactions, is a fundamental problem in strongly correlated electron systems. By the diffusive quantum Monte Carlo method (DQMC), the critical electron density for crystallization is obtained as $r_s = r_0/a_B^* \simeq 150$ for a three-dimensional electron gas ($r_0 = (\pi n_e)^{-1/2}$, a_B^* : the effective Bohr radius) [1]. The critical value of r_s is lowered down to $r_s \simeq 31$ for a two-dimensional electron gas [2, 3]. In addition to the Coulomb interaction, the lattice commensurability reduces the critical Coulomb interaction for crystallization [4].

In this work, we studied the Wigner crystallization in spinless Fermion systems on a square lattice at finite fillings by highly accurate simulation based on the many-variable variational Monte Carlo (mVMC) method [5]. By performing the calculations up to the order of 10^3 sites, we determine the transition points for $n = 2, 4, 8, 12, 16$ and draw the phase diagram as functions of r_s and $1/n$ as shown in Fig. 1.

In contrast to the previous works by path-integral renormalization group (PIRG) [4], we found that the transition points at finite fillings becomes significantly small. Nevertheless, the transition points seem to continuously connect to its continuum limits, which is consistent with the previous works. We also examined the nature of the associated metal-insulator transition by calculation the momentum distribution

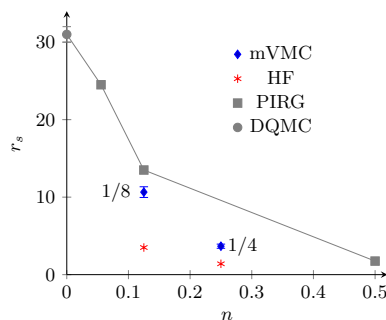


Figure 1: Phase diagram in the plane of the electron-density and r_s . We also show the result of the Hartree-Fock (HF) approximation.

and the charge gap [6].

References

- [1] D. M. Ceperley and B. J. Alder, Phys. Rev. Lett. **45**, 566 (1980).
- [2] M. Imada and M. Takahashi, J. Phys. Soc. Jpn. **53**, 3770 (1984).
- [3] N. D. Drummond and R. J. Needs, Phys. Rev. Lett. **102**, 126402 (2009).
- [4] Y. Noda and M. Imada, Phys. Rev. Lett. **89**, 176803 (2002).
- [5] T. Misawa, et al., Comput. Phys. Commun. **235**, 447 (2019).
- [6] M. K. Ritter, K. Ido, T. Misawa, and T. Kato, in preparation.

Magnetic and transport properties in double-exchange systems with quasiperiodicity

Akihisa Koga

Department of Physics, Tokyo Institute of Technology, Meguro, Tokyo 152-8551

Quasicrystals (QCs) have no translational symmetry but possess long-range order and special rotational symmetry. Since its first discovery in 80's, intensive efforts have been made to search various type of QC materials and to reveal characteristic features. In this decade, there have been several important experimental findings in QC materials, which include quantum critical behaviors in Au-Al-Yb alloy and the emergence of superconductivity in Al-Zn-Mg QC alloy. These experiments suggest important roles of electronic correlations in these materials, and stimulate theoretical studies of the correlation and induced ordered phases in QC systems.

Motivated by this situation, we have studied possibility of the excitonic insulating (EI) state in the two-band Hubbard model [1] and the magnetism of the double exchange model [2] on the Penrose lattice. In the former study [1], we considered the vertex model and the center model on the Penrose lattice to determine their ground state phase diagram in terms of the real-space mean-field theory. We have revealed the existence of the stable EI phase induced by small interband interactions [Fig. 1(a)]. We pointed out that this originates from the electron-hole pairing for the completely or nearly degenerated states, which is characteristic of the QC systems. In addition, we also discussed the spatial structure of the order in terms of the so-called perpendicular space [Fig. 1(b)]. In the second study [2], we investigated the double exchange model on the Penrose lattice in terms of a Monte Carlo method. We showed the existence of the ferromagnetism and revealed that its general fea-

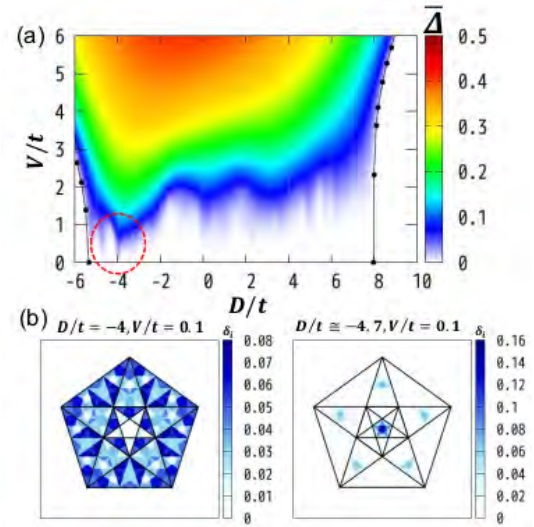


Figure 1: (a) EI order parameter of the two-band Hubbard model of the center model on the Penrose lattice. Red dotted circles indicates the stable EI states with small interactions. (b) Analysis in the perpendicular space for the stable EI phases.

tures such as temperature dependence resemble those of the system on the normal square lattice. By means of the analysis in the perpendicular space, we discussed the characteristic real-space structure of the magnetism in this QC system.

References

- [1] K. Inayoshi, Y. Murakami, and A. Koga: arXiv:2002.05870 (2020).
- [2] Y. Takeuchi, Master thesis, Tokyo Institute of Technology (2020. Mar).

Numerical analysis for nonequilibrium dynamics in correlated electron systems with orbital degrees of freedom

Akihisa Koga

Department of Physics, Tokyo Institute of Technology, Meguro, Tokyo 152-8551

Strongly correlated systems with orbital degrees of freedom can lead to intriguing spin systems. One of the important examples is the Kitaev quantum spin model, which consists of anisotropic exchange couplings on the honeycomb lattice and shows the quantum spin liquid (QSL) state at low temperatures. Although the Kitaev model was originally proposed theoretically, it is considered to be realized in α - RuCl_3 , and other strongly correlated systems such as A_2IrO_3 ($\text{A} = \text{Na}, \text{Li}$) are also candidates of the Kitaev QSL. So far, the static properties in the Kitaev QSL have been the main focus of this field and many characteristic features such as the fractionalization of specific heats and the thermal Hall effects have been reported. Thus, a simple question naturally arises what is the characteristic dynamical properties of the Kitaev QSL.

Motivated by this, we studied the spin transport through the QSL by investigating the real-space dynamics of the $S = 1/2$ Kitaev system with a zigzag edge structure [2] [Fig.1(a)]. We followed the dynamics after the magnetic field pulse applied to one of the edges with the time-dependent Majorana mean-field theory and the exact diagonalization. We showed that, although no spin moments are induced in the Kitaev QSL region, the spin moments are excited in the opposite edge region [Fig.1(b)]. We revealed that this anomalous spin transport originates from the fractionalization of the spins in the Kitaev QSL into the itinerant and localized Majorana fermions. Namely, after the excitation, only the itinerant Majorana fermions can propagate through the QSL, hence the magnetization is absent there. When the itinerant Majorana reaches

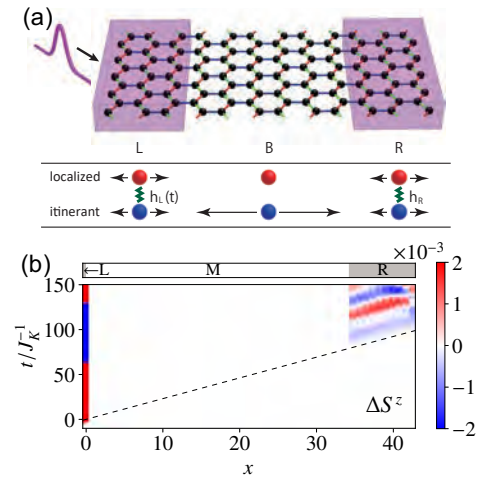


Figure 1: (a) Schematic pictures of our setup and the process involved in the anomalous spin transport. (b) the mean-field result of the spin dynamics of the Kitaev model.

the other edge under the static magnetic field, the hybridization between the local Majorana fermions yields the finite spin momentum. We also studied the $S = 1$ Kitaev model to show the existence of the similar anomalous spin transport [3].

References

- [1] A. Kitaev: *Ann. Phys.* **321** (2006) 2.
- [2] T. Minakawa, Y. Murakami, A. Koga and J. Nasu: arXiv:1912.10599 (2019).
- [3] A. Koga, T. Minakawa, Y. Murakami and J. Nasu: *J. Phys. Soc. Jpn.* **89** (2020) 033701.

Novel topological phenomena induced by strongly correlated dynamics

Tsuneya YOSHIDA

*Department of Physics, University of Tsukuba
Tsukuba, Ibaraki 305-8571*

Focusing on non-Hermitian topological phenomena, we have analyzed correlated systems. Specifically, we have analyzed exceptional band touching for quasi-particle spectrum of correlated systems in equilibrium [1, 2, 3]. Our works [1, 3] have discovered novel exceptional band touching which we dub symmetry-protected exceptional rings (surfaces) in two (three) dimensions, respectively. In addition, we have also elucidated that for Kondo insulators, such non-Hermitian band touching emerges around Kondo temperatures. Furthermore, focusing on dynamics of open quantum systems with two-body loss, we have discovered a non-Hermitian fractional quantum Hall state (see Fig. 1), which extends the non-Hermitian physics to long range entangled states. The above set up is relevant to the cold atoms with two-body loss.

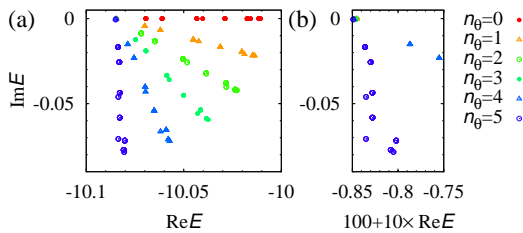


Figure 1: (Color Online). Energy spectrum of non-Hermitian Hamiltonian. Panel (b) is the magnified version of the range in $-10.085 < \text{Re}E < -10.075$.

In addition to the above works on non-Hermitian systems, we have addressed topology with crystalline effects [5, 6]. In par-

ticular, we have found that mirror symmetry and non-Hermitian topology induces novel skin effect protected by mirror symmetry which may be realized for an electric circuit composed of negative impedance converters. Besides that we have elucidated the other topological phases protected by crystalline symmetry [7, 8, 9]. For instance, we have extended the notion of higher order topology to correlated systems, which discovered a new topological state, a higher-order topological Mott insulating state [9]. We also have proposed an efficient method to compute Z_4 topological invariant for glide symmetric systems [7].

References

- [1] Kazuhiro Kimura, Tsuneya Yoshida, and Norio Kawakami: Phys. Rev. B **100**, 115124 (2019).
- [2] Yoshihiro Michishita, Tsuneya Yoshida, and Robert Peters: Phys. Rev. B **101**, 085122.
- [3] Tsuneya Yoshida, Robert Peters, Norio Kawakami, Yasuhiro Hatsugai: arXiv:2002.11265.
- [4] Tsuneya Yoshida, Koji Kudo, and Yasuhiro Hatsugai: Sci. Rep. **9**, 16895 (2019).
- [5] Tsuneya Yoshida and Yasuhiro Hatsugai: Phys. Rev. B **100**, 054109 (2019).

- [6] Tsuneya Yoshida, Tomonari Mizoguchi, and Yasuhiro Hatsugai: arXiv:1912.12022.
- [7] Tsuneya Yoshida, Akito Daido, Norio Kawakami, and Youichi Yanase: Phys. Rev. B **99**, 235105 (2019).
- [8] Kazuhiro Kimura, Tsuneya Yoshida, and Norio Kawakami: JPS Conf. Proc. **30**, 011012 (2020).
- [9] Koji Kudo, Tsuneya Yoshida, and Yasuhiro Hatsugai: Phys. Rev. Lett. **123**, 196402 (2019).

Two-Channel Kondo Effect Emerging in a Multiorbital Anderson Model Hybridized with Γ_7 and Γ_8 Conduction Bands

Takashi HOTTA

*Department of Physics, Tokyo Metropolitan University
1-1 Minami-Osawa, Hachioji, Tokyo 192-0397*

To explore the emergence of a quantum critical point (QCP) between non-Fermi-liquid and Fermi-liquid phases, we investigate the states in the vicinity of two-channel Kondo phase. For the purpose, we analyze a seven-orbital impurity Anderson model hybridized with three conduction bands (one Γ_7 and two Γ_8) by employing a numerical renormalization group (NRG) method.

First we consider one f -electron state, which is the eigenstate of spin-orbit and crystalline electric field (CEF) potential terms. Under the cubic CEF potential, we obtain Γ_7 doublet and Γ_8 quartet from $j = 5/2$ sextet, whereas we find Γ_6 doublet, Γ_7 doublet, and Γ_8 quartet from $j = 7/2$ octet. By using those one-electron state as bases, we describe the local f -electron Hamiltonian as

$$\begin{aligned}
 H_{\text{loc}} = & \sum_{j,\mu,\tau} (\lambda_j + B_{j,\mu} + E_f) f_{j\mu\tau}^\dagger f_{j\mu\tau} \\
 & + \sum_{j_1 \sim j_4} \sum_{\mu_1 \sim \mu_4} \sum_{\tau_1 \sim \tau_4} I_{\mu_1 \tau_1 \mu_2 \tau_2, \mu_3 \tau_3 \mu_4 \tau_4}^{j_1 j_2, j_3 j_4} \quad (1) \\
 & \times f_{j_1 \mu_1 \tau_1}^\dagger f_{j_2 \mu_2 \tau_2}^\dagger f_{j_3 \mu_3 \tau_3} f_{j_4 \mu_4 \tau_4},
 \end{aligned}$$

where $f_{j\mu\tau}$ denotes the annihilation operator of a localized f electron in the bases of (j, μ, τ) , j is the total angular momentum, $j = 5/2$ and $7/2$ are denoted by “ a ” and “ b ”, respectively, μ distinguishes the cubic irreducible representation, Γ_8 states are distinguished by $\mu = \alpha$ and β , while Γ_7 and Γ_6 states are labeled by $\mu = \gamma$ and δ , respectively, τ is the pseudo-spin which distinguishes the degeneracy concerning

the time-reversal symmetry, and E_f is the f -electron level to control the local f -electron number at an impurity site.

As for the spin-orbit coupling term, we obtain $\lambda_a = -2\lambda$ and $\lambda_b = (3/2)\lambda$, where λ is the spin-orbit coupling of f electron. For Pr ion, we set $\lambda = 0.1\text{eV}$ in this research. Concerning the CEF potential term for $j = 5/2$, we obtain $B_{a,\alpha} = B_{a,\beta} = 1320B_4^0/7$ and $B_{a,\gamma} = -2640B_4^0/7$, where B_4^0 denotes the fourth-order CEF parameter for the angular momentum $\ell = 3$. Note that the sixth-order CEF potential term B_6^0 does not appear for $j = 5/2$, since the maximum size of the change of the total angular momentum is less than six. On the other hand, for $j = 7/2$, we obtain $B_{b,\alpha} = B_{b,\beta} = 360B_4^0/7 + 2880B_6^0$, $B_{b,\gamma} = -3240B_4^0/7 - 2160B_6^0$, and $B_{b,\delta} = 360B_4^0 - 3600B_6^0/7$. Note also that B_6^0 term appears in this case. In the present calculations, we treat B_4^0 and B_6^0 as parameters.

The matrix element of the Coulomb interaction is expressed by I . Here we do not show the list for the explicit forms of I , but they are expressed with the use of four Slater-Condon parameters, F^0 , F^2 , F^4 , and F^6 . Although the Slater-Condon parameters of a material should be determined from experimental results, here we simply set the ratio as $F^0/10 = F^2/5 = F^4/3 = F^6 = U$, where U is the Hund’s rule interaction among f orbitals. It is reasonable to set U as 1 eV in this research.

In Fig. 1, we show the local CEF ground-

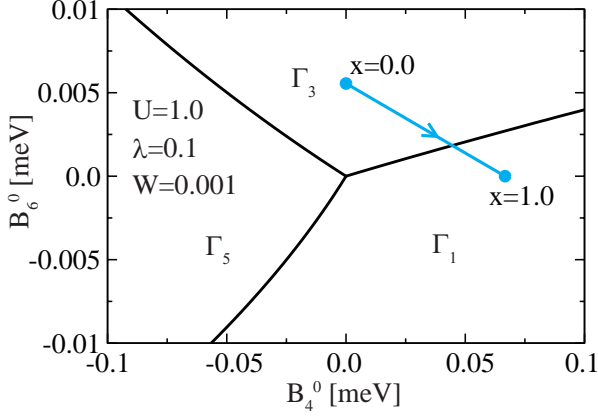


Figure 1: Local CEF ground-state phase diagram on the plane of (B_4^0, B_6^0) for $n = 2$. The line is given by $B_4^0 = Wx/15$ and $B_6^0 = W(1 - |x|)/180$ with $W = 10^{-3}$.

state phase diagram for $n = 2$, obtained from the diagonalization of H_{loc} . For $n = 2$, the ground-state multiplet for $B_4^0 = B_6^0 = 0$ is characterized by total angular momentum $J = 4$. Under the cubic CEF potentials, the nonet of $J = 4$ is split into four groups as Γ_1 singlet, Γ_3 doublet, Γ_4 triplet, and Γ_5 triplet. Among them, Γ_4 triplet does not appear as a solo ground state under the cubic CEF potential with O_h symmetry.

Now we include the Γ_7 and Γ_8 conduction electron bands. Here we consider only the hybridization between conduction and $j = 5/2$ electrons. The Hamiltonian is given by

$$H = \sum_{\mathbf{k}, \mu, \tau} \varepsilon_{\mathbf{k}} c_{\mathbf{k}\mu\tau}^\dagger c_{\mathbf{k}\mu\tau} + \sum_{\mathbf{k}, \mu, \tau} V_\mu (c_{\mathbf{k}\mu\tau}^\dagger f_{a\gamma\tau} + \text{h.c.}) + H_{\text{loc}}, \quad (2)$$

where $\varepsilon_{\mathbf{k}}$ is the dispersion of conduction electron with wave vector \mathbf{k} , $c_{\mathbf{k}\gamma\tau}$ is an annihilation operator of conduction electrons, and V_μ denotes the hybridization between f electron in the μ orbital and conduction electron of the μ band. Here we set $V_\alpha = V_\beta = V_\gamma = V$.

In this research, we analyze this model by employing the NRG method [1]. We introduce a cut-off Λ for the logarithmic discretization of the conduction band. Due to the limitation of computer resources, we keep M low-energy

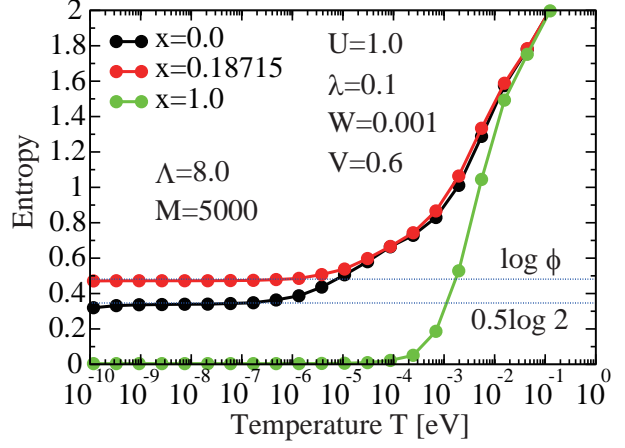


Figure 2: Entropies vs. temperature for $x = 0$, 0.18715, and 1 with $W = 10^{-3}$.

states. Here we use $\Lambda = 8$ and $M = 5,000$. Note that the temperature T is defined as $T = D\Lambda^{-(N-1)/2}$ in the NRG calculation, where N is the number of the renormalization step and D is a half of conduction band width. Here we set $D = 1$ eV.

In Fig. 2, we show the calculation results for entropies, when we change the local CEF states from Γ_3 doublet ($x = 0$) to Γ_1 singlet ($x = 1$) on the line in Fig. 1. For $x = 0$, we find an entropy of $0.5 \log 2$ at low temperatures, indicating the two-channel Kondo state (non-Fermi-liquid phase), while for $x = 1$, we obtain the CEF singlet state (Fermi-liquid phase). After repeating the NRG calculations, at $x = 0.18715$, we find an entropy plateau of $\log \phi$ with $\phi = (\sqrt{5} + 1)/2$. This is the same as the residual entropy for the three-channel Kondo effect. We consider that the entropy $\log \phi$ suggests the emergence of QCP between non-Fermi-liquid and Fermi-liquid phases. Details will be discussed elsewhere in future [2].

References

- [1] H. R. Krishna-murthy, J. W. Wilkins, and K. G. Wilson, Phys. Rev. B **21**, 1003 (1980).
- [2] T. Hotta, in preparation.

Research of Two-Channel Kondo Effect in Transuranium Systems

Dai MATSUI and Takashi HOTTA

*Department of Physics, Tokyo Metropolitan University
1-1 Minami-Osawa, Hachioji, Tokyo 192-0397*

On the basis of the electron-hole relation between f^2 and f^4 states in a j - j coupling scheme, we hit upon an idea that two-channel Kondo phenomena can be observed even in cubic transuranium compounds including Np and Pu ions with local Γ_3 non-Kramers doublet ground state. To clarify this point, we analyze a seven-orbital impurity Anderson model hybridized with degenerate Γ_8 conduction electron bands by employing a numerical renormalization group (NRG) method [1].

The model Hamiltonian is given by

$$\begin{aligned}
 H = & \sum_{\mathbf{k}, \mu, \tau} \varepsilon_{\mathbf{k}} c_{\mathbf{k}\mu\tau}^\dagger c_{\mathbf{k}\mu\tau} + \sum_{\mathbf{k}, \mu, \tau} V (c_{\mathbf{k}\mu\tau}^\dagger f_{a\mu\tau} + \text{h.c.}) \\
 & + \sum_{j, \mu, \tau} (\lambda_j + B_{j, \mu} + E_f) f_{j\mu\tau}^\dagger f_{j\mu\tau} \\
 & + \sum_{j_1 \sim j_4} \sum_{\mu_1 \sim \mu_4} \sum_{\tau_1 \sim \tau_4} I_{\mu_1 \tau_1 \mu_2 \tau_2, \mu_3 \tau_3 \mu_4 \tau_4}^{j_1 j_2, j_3 j_4} \\
 & \times f_{j_1 \mu_1 \tau_1}^\dagger f_{j_2 \mu_2 \tau_2}^\dagger f_{j_3 \mu_3 \tau_3} f_{j_4 \mu_4 \tau_4},
 \end{aligned} \tag{1}$$

where $\varepsilon_{\mathbf{k}}$ denotes the energy of Γ_8 conduction electron with wave vector \mathbf{k} , $c_{\mathbf{k}\mu\tau}$ indicates the annihilation operator of Γ_8 conduction electron, μ distinguishes the cubic irreducible representation, Γ_8 states are distinguished by $\mu = \alpha$ and β , while Γ_7 and Γ_6 states are labeled by $\mu = \gamma$ and δ , respectively, τ is the pseudo-spin which distinguishes the degeneracy concerning the time-reversal symmetry, V is the hybridization between conduction and localized electrons, $f_{j\mu\tau}$ indicates the annihilation operator of a localized f electron in the bases of (j, μ, τ) , j is the total angular momentum, $j = 5/2$ and $7/2$ are denoted by “a” and “b”, respectively, and E_f is the f -electron

level to control the local f -electron number at an impurity site. In the present case, we consider the hybridization between Γ_8 conduction electrons and the Γ_8 quartet of $j = 5/2$.

As for the spin-orbit coupling term, we obtain $\lambda_a = -2\lambda$ and $\lambda_b = (3/2)\lambda$, where λ is the spin-orbit coupling of f electron. The magnitude of λ depends on the kind of actinide atoms, but in this research, we set $\lambda = 0.3$ eV, since we consider Np and Pu ions. Concerning the CEF potential term for $j = 5/2$, we obtain $B_{a, \alpha} = B_{a, \beta} = 1320B_4^0/7$ and $B_{a, \gamma} = -2640B_4^0/7$, where B_4^0 denotes the fourth-order CEF parameter for the angular momentum $\ell = 3$. Note that the sixth-order CEF potential term B_6^0 does not appear for $j = 5/2$, since the maximum size of the change of the total angular momentum is less than six. On the other hand, for $j = 7/2$, we obtain $B_{b, \alpha} = B_{b, \beta} = 360B_4^0/7 + 2880B_6^0$, $B_{b, \gamma} = -3240B_4^0/7 - 2160B_6^0$, and $B_{b, \delta} = 360B_4^0 - 3600B_6^0/7$. Note also that B_6^0 terms appear in this case. In the present calculations, we treat B_4^0 and B_6^0 as parameters.

The matrix element of the Coulomb interaction is expressed by I . To save space, we do not show the explicit forms of I here, but they are expressed by four Slater-Condon parameters (F^0, F^2, F^4, F^6) and Gaunt coefficients. As for the magnitudes of Slater-Condon parameters, first we set $F^0 = 10$ eV by hand. Others are determined so as to reproduce excitation spectra of U^{4+} ion with two $5f$ electrons. The results are $F^2 = 6.4$ eV, $F^4 = 5.6$

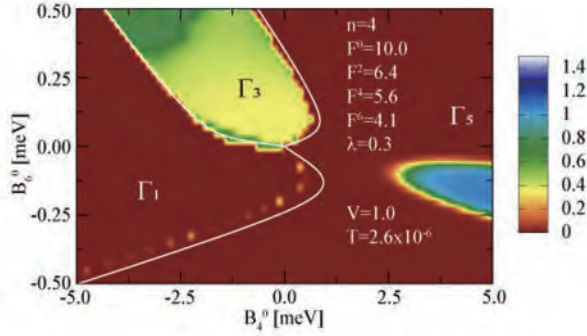


Figure 1: Color contour map of the entropy for $n = 4$ on the plane of (B_4^0, B_6^0) for $V=1.0$ and $T = 2.6 \times 10^{-6}$. White curves denote the boundaries among local CEF ground states.

eV, and $F^6 = 4.1$ eV [2].

In this research, we analyze the model by employing the NRG method [3]. We introduce a cut-off Λ for the logarithmic discretization of the conduction band. Due to the limitation of computer resources, we keep M low-energy states. Here we use $\Lambda = 5$ and $M = 2,500$. Note that the temperature T is defined as $T = D\Lambda^{-(N-1)/2}$ in the NRG calculation, where N is the number of the renormalization step and D is a half of conduction band width. We set $D = 1$ eV in this research.

In Fig. 1, we show the contour color map of the entropy on the plane of (B_4^0, B_6^0) for $V = 1.0$ and $T = 2.6 \times 10^{-6}$. To visualize precisely the behavior of entropy, we define the color of the entropy between 0 and 1.5, as shown in the right color bar. Note that the green and yellow regions indicate the entropy of $\log 2$ and $0.5 \log 2$, respectively. We immediately notice that a region with an entropy of $0.5 \log 2$ (yellow region) almost corresponds to that of the Γ_3 CEF ground state. Note that for large B_6^0 , the color becomes green, but when we decrease the temperature, we find the entropy of $0.5 \log 2$ even for large B_6^0 . The results strongly suggest the emergence of quadrupole two-channel Kondo effect for the case of $n = 4$. Note that in the present model, we have observed the discontinuous change in entropy behavior between yellow (Γ_3) and red

(Γ_1 or Γ_5) regions. Quantum critical behavior which may occur between non-Fermi-liquid and Fermi-liquid phases will be discussed elsewhere in future.

Here we remark that there exists a blue region corresponding to $\log 3$ in the local Γ_5 state. This is quite natural, since the local Γ_5 state is triply degenerate. The Γ_5 moment is screened by Γ_8 conduction electrons and thus, it is expected that the conventional Kondo effect occurs in the Γ_5 region, although the magnitude of the Kondo temperature significantly depends on the hybridization and excitation energy.

Note also that in the region of $B_6^0 < 0$, we observe some blurry yellow spots along the boundary curve between Γ_1 singlet and Γ_5 triplet local ground states. The QCP is known to appear between the CEF and Kondo singlet states for $n = 2$ [4]. Thus, we deduce that those spots form a QCP curve, although we could not obtain enough amounts of numerical results to depict the smooth curve here.

Finally, we provide a brief comment on actual materials to observe the two-channel Kondo effect for the case of $n = 4$. In rare-earth ions, the case of $n = 4$ corresponds to Pm^{3+} , but unfortunately, there exist no stable isotopes for Pm. Thus, we turn our attention to actinide ions such as Np^{3+} and Pu^{4+} with $5f^4$ configurations. It may be difficult to synthesize new Np and Pu compounds, but we expect that Np 1-2-20 compound will be synthesized in future.

References

- [1] D. Matsui and T. Hotta, JPS Conf. Proc. **30**, 011125 (2020).
- [2] T. Hotta, Phys. Rev. B **80**, 024408 (2009).
- [3] H. R. Krishna-murthy, J. W. Wilkins, and K. G. Wilson, Phys. Rev. B **21**, 1003 (1980).
- [4] T. Hotta, Physica B **536**, 203 (2018).

First-principles and quantum many-body calculations for electronic states and superconductivity in the multi-band systems

Yoshiaki ŌNO

*Department of Physics, Niigata University
Ikarashi, Nishi-ku, Niigata, 950-2181*

Tungsten bronzes $A_x\text{WO}_3$ ($A=\text{Na, K, Rb, Cs}$) are known to show the superconductivity for $0.15 < x < 0.35$, where the superconducting transition temperature T_c is found to increase rapidly with decreasing x up to 7K. In addition, at further low doping $x \sim 0.05$, remarkable high- T_c superconductivities are reported at $T_c=91\text{K}$ for $A=\text{Na}$ and $T_c=120\text{K}$ for $A=\text{H}$. The systems also show rich structural phases such as cubic for $x > 0.4$, tetragonal for $0.1 < x < 0.4$, orthorhombic for $0.03 < x < 0.1$ and monoclinic for $x < 0.03$, which are well accounted for by the first-principles calculations. However, the superconductivity in which the structural phases and those transitions are considered to play important roles for determining T_c was not discussed there. The purpose of this work is to study the superconductivity in $A_x\text{WO}_3$ on the basis of the first-principles calculation and to discuss the effect of the ferro-orbital fluctuation which is found to be largely enhanced around the structural phase transition and is expected to induce the pairing interaction as previously discussed in the iron-based superconductivity.

We calculate T_c on the basis of the first-principles calculation by using Quantum ESPRESSO and find that the x dependence of T_c is qualitatively consistent with the experiments. The significant x dependence of T_c is mainly due to that of the electron-phonon coupling constant λ which decreases with increasing x because of the screening effect as

discussed by several authors. However, the calculated value of T_c is considerably smaller than the experimental values, and hence the pairing interaction mediated by the electronic fluctuation such as the orbital fluctuation is expected to be responsible for the pairing mechanism in addition to the BCS phonon mechanism which is exclusively taken into account in the present first-principles calculation. Then, we also calculate the pairing interaction on the basis of the effective three band model consists of $W-t_{2g}$ orbitals by taking into account of the Jahn-Teller electron-phonon coupling within the random phase approximation and find that the pairing interaction is largely enhanced due to the ferro-orbital fluctuation which becomes large around the structural phase transition[1].

Recently, the Pr 1-2-20 systems $\text{PrT}_2\text{X}_{20}$ have been intensively investigated concerning their specific features including quadrupole orders, superconductivity and non-Fermi liquid behaviors. The crystalline electric field ground states of the Pr ions are the non-Kramers doublets Γ_{23} which have the electric quadrupole moments with no magnetic moment. In fact, $\text{PrTi}_2\text{Al}_{20}$ and $\text{PrV}_2\text{Al}_{20}$ exhibit the ferro-quadrupole (FQ) and the antiferro-quadrupole (AFQ) orders, respectively. They also show remarkable superconductivities coexisting with the quadrupole orders. To discuss the quadrupole order and the superconductivity, the details of the energy bands and the Fermi surfaces are important. In the Pr

1-2-20 systems, the de Haas-van Alphen experiments revealed that the Fermi surfaces are well accounted for by the first-principles band calculations for the corresponding La 1-2-20 systems, indicating that the Pr 4f electrons are sufficiently localized. Therefore, the quadrupole orders are considered due to the Ruderman-Kittel-Kasuya-Yosida (RKKY) interaction between the quadrupole moments of the localized Pr 4f electrons. The purpose of this study is to evaluate the RKKY interaction on the basis of the realistic energy band structure extracted from the first-principles calculation and to discuss the quadrupole orders in $\text{PrTi}_2\text{Al}_{20}$ and $\text{PrV}_2\text{Al}_{20}$.

We perform the first-principles calculations for $\text{LaT}_2\text{Al}_{20}$ ($T=\text{Ti, V}$) by using WIEN2k code where we also employ the GGA+ U method with $U = 60\text{eV}$ to exclude the La-4f components near the Fermi level. The obtained Fermi surfaces of $\text{LaTi}_2\text{Al}_{20}$ are in good agreement with those in the previous study. Then, we construct the tight-binding model for the conduction electrons so as to reproduce the electronic structure near the Fermi level by using the maximally localized Wannier functions which consist of 196 orbitals: La- d (5 orbitals \times 2 sites), La- s (1 orbital \times 2 sites), T- d (5 orbitals \times 4 sites), T- s (1 orbital \times 4 sites), Al- p (3 orbitals \times 40 sites) and Al- s (1 orbital \times 40 sites) in the conventional unit cell. Based on the effective model, we calculate the quadrupole susceptibility of the conduction electrons and then evaluate the RKKY interaction mediated by the conduction electrons. The obtained results indicate that the wave vectors of the expected quadrupole orders are $Q = (0, 0, 0)$ (FQ) for $\text{PrTi}_2\text{Al}_{20}$ and $Q = (\pi/a, \pi/a, 0)$ (AFQ) for $\text{PrV}_2\text{Al}_{20}$, respectively, as consistent with the experiments[2].

Quasicrystals first discovered by Shechtman *et al.* in Al-Mg alloy have been extensively investigated as they show various anomalous properties due to their specific structures which are not periodic but have kinds of trans-

lational orders with the 5-fold (8-, 10- and 12-fold) rotational symmetry. Recently, the bulk superconductivity at a transition temperature $T_c \sim 0.05\text{K}$ has been discovered by Kamiya *et al.* in the Al-Mg-Zn quasicrystal and its approximant, where the basic cluster is considered to be the Bergman-type cluster, and has attracted much attention for its symmetry and pairing mechanism. As for the theoretical study, the $\text{Al}_{30}\text{Mg}_{40}\text{Zn}_{30}$ 1/1 approximant was previously studied on the basis of the first-principles calculation and the origin of the pseudo gap near the Fermi level was discussed. However, the electronic state with the composition ratio corresponding to the superconducting compound was not discussed there. Then, we perform the first-principles calculations (OpenMX code) for the Al-Mg-Zn 1/1 approximants with various composition ratios including the superconducting one and find that the over-all structure of the density of states seems to be almost independent of the composition ratio but the energy band dispersions near the Fermi level and the Fermi surfaces are largely dependent on the composition ratio. On the basis of the obtained electronic states, we also discuss the possible superconductivity[3].

References

- [1] Takuya Sekikawa, Rai Watabe, Jun Ishizuka, Yoshihiro Nitta, Kazuhiro Sano and Yoshiaki Ōno, JPS Conf. Proc. **30**, 011043 (2020).
- [2] Yuto Iizuka, Takemi Yamada, Katsurou Hanzawa and Yoshiaki Ōno, JPS Conf. Proc. **30**, 011152 (2020).
- [3] Masaki Saito, Takuya Sekikawa and Yoshiaki Ōno, *14th International Conference on the Structure of Non-Crystalline Materials* (NCM14).

Search for new types of skyrmion crystals based on point group symmetry

Satoru Hayami

Department of Applied Physics, The University of Tokyo, Tokyo 113-8656

Multiple- Q magnetic states, which are characterized as a superposition of different wave vectors, open a new path toward applications to next-generation electronics and spintronics device in condensed matter physics. Amongst them, the superposition of spiral states gives rise to unconventional noncollinear and non-coplanar magnetic textures, such as the magnetic vortex crystal and magnetic skyrmion crystal, which become a source of unconventional topological excitations and transport properties [1]. Especially, since the discovery of the magnetic skyrmions in noncentrosymmetric magnets, their studies have been extensively done in both theory and experiments.

Meanwhile, recent theoretical studies point out the emergence of the skyrmion crystals in centrosymmetric Mott insulators. They are stabilized by taking into account various factors, such as frustrated exchange interactions and thermal fluctuations [2, 3, 4, 5]. Moreover, another interesting situation is brought by considering the interplay between itinerant electrons and localized spins. There, effective long-ranged interactions mediated through itinerant electrons play an important role in stabilizing the skyrmion and vortex crystals [6, 7, 8], which might provide a deep understanding of the microscopic mechanism of the multiple- Q skyrmion, vortex, and hedgehog crystals found in d - and f -electron materials.

In this project, we investigate the skyrmion physic in itinerant magnets by considering an anisotropic magnetic interaction [9]. We start from the Kondo lattice model with

the anisotropic xxz -type spin-charge coupling. The Hamiltonian is represented by

$$\begin{aligned} \mathcal{H} = & - \sum_{i,j,\sigma} t_{ij} c_{i\sigma}^\dagger c_{j\sigma} + J_z \sum_{i,\sigma,\sigma'} \sigma_{\sigma\sigma'}^z S_i^z c_{i\sigma}^\dagger c_{i\sigma'} \\ & + J_{xy} \sum_{i,\sigma,\sigma'} (\sigma_{\sigma\sigma'}^x S_i^x + \sigma_{\sigma\sigma'}^y S_i^y) c_{i\sigma}^\dagger c_{i\sigma'}, \quad (1) \end{aligned}$$

where $c_{i\sigma}^\dagger$ and $c_{i\sigma}$ are creation and annihilation operators of an itinerant electron at site i and spin σ , respectively. The first term represents the hopping of itinerant electrons and the second and third terms denote the spin-charge coupling where $|\mathbf{S}_i| = 1$ and $\boldsymbol{\sigma}$ is the Pauli matrix. J_{xy} and J_z are the anisotropic coupling constants for xy and z spin components, respectively.

We derive an effective spin model in Eq. (1) by assuming (i) the weak-coupling regime for $J_{xy}, J_z \ll W$ (W is the bandwidth) and (ii) the multiple peak structures of the bare magnetic susceptibility. Then, the spin model is obtained as

$$\mathcal{H} = -2 \sum_{\nu=1-3} (\tilde{J}\Gamma_{\mathbf{Q}_\nu} + \tilde{K}\Gamma_{\mathbf{Q}_\nu}^2), \quad (2)$$

where $\Gamma_{\mathbf{Q}_\nu} = \sqrt{1-A^2}(S_{\mathbf{Q}_\nu}^x S_{-\mathbf{Q}_\nu}^x + S_{\mathbf{Q}_\nu}^y S_{-\mathbf{Q}_\nu}^y) + AS_{\mathbf{Q}_\nu}^z S_{-\mathbf{Q}_\nu}^z$. We adopt a triangular lattice with six peaks in the bare susceptibility: $\pm\mathbf{Q}_1 = \pm(\pi/3, 0)$, $\pm\mathbf{Q}_2 = \pm(-\pi/6, \sqrt{3}\pi/6)$, and $\pm\mathbf{Q}_3 = \pm(-\pi/6, -\sqrt{3}\pi/6)$. The first term represents the bilinear interaction with $\tilde{J} = 1$ and the second term represents the biquadratic interaction with the positive coupling constant $\tilde{K} = K/N > 0$ (N is the number of spins). The former originates from the

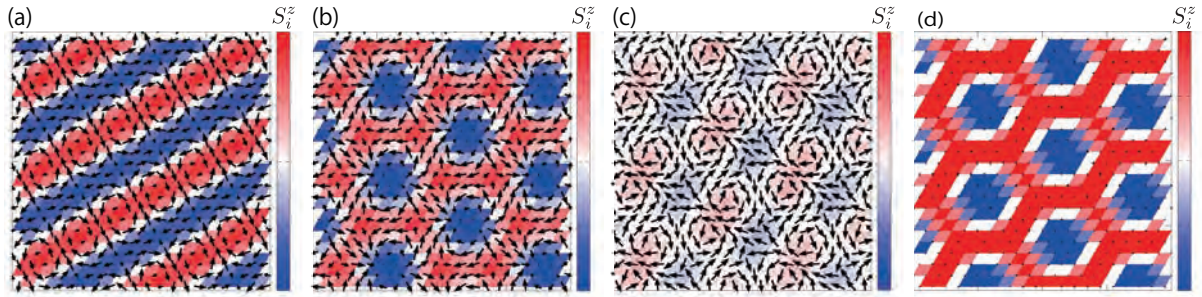


Figure 1: Snapshots of the spin configurations (see the text). The arrows represent the xy component and the contour shows the z component of the spin moment.

second-order perturbation, while the latter arises from the fourth-order perturbation. The magnetic anisotropy is represented by A ; $0 \leq A < 1/\sqrt{2}$ for the easy-axis interaction and $1/\sqrt{2} < A \leq 1$ for the easy-plane interaction.

The magnetic phase diagram of the effective spin model in Eq. (2) is investigated by performing simulated annealing from high temperature. We apply the Metropolis local updates under periodic boundary conditions in both directions for the 96^2 spins. To find the optimal spin configurations, we gradually reduce the temperature with the rate $T_{n+1} = \alpha T_n$, where T_n is the temperature in the n th step. We start from the initial temperature $T_0 = 10^{-1}$ - 10^0 . We typically set $\alpha \sim 0.99999$ and the final temperature $T = 10^{-4}$ - 10^{-3} .

As a result, we find several magnetic ordered states with a net scalar chirality including the skyrmion and vortex crystals by constructing the ground-state phase diagram in a wide range of model parameters. We show that two types of the skyrmion crystal phases with the topological number of two are realized for large K : one is identified as the superposition of the magnetic vortex structures in the xy spin component and the sinusoidal wave in the z spin component [Fig. 1(a)] and the other is denoted as the bubble-type magnetic configurations satisfying the sixfold rotational symmetry in both xy and z spin components [Fig. 1(b)]. We also find a triple- Q

state with a finite net scalar chirality, which is different from the skyrmion crystal by increasing the easy-plane anisotropic interaction [Fig. 1(c)]. Moreover, we find that the strong easy-axis anisotropic interaction gives rise to the triple- Q magnetic bubble crystal with the collinear z spin component [Fig. 1(d)].

References

- [1] N. Nagaosa, Y. Tokura, *Nat. Nanotech.* **8** (12) (2013) 899–911.
- [2] T. Okubo, S. Chung, H. Kawamura, *Phys. Rev. Lett.* **108** (2012) 017206.
- [3] A. O. Leonov, M. Mostovoy, *Nat. Commun.* **6** (2015) 8275.
- [4] S.-Z. Lin, S. Hayami, *Phys. Rev. B* **93** (2016) 064430.
- [5] S. Hayami, S.-Z. Lin, C. D. Batista, *Phys. Rev. B* **93** (2016) 184413.
- [6] Y. Akagi, M. Udagawa, Y. Motome, *Phys. Rev. Lett.* **108** (2012) 096401.
- [7] R. Ozawa, S. Hayami, K. Barros, G.-W. Chern, Y. Motome, C. D. Batista, *J. Phys. Soc. Jpn.* **85** (10) (2016) 103703.
- [8] S. Hayami, R. Ozawa, Y. Motome, *Phys. Rev. B* **95** (2017) 224424.
- [9] S. Hayami, submitted.

Multipole and anisotropic superconductivity from first-principles

Jun Ishizuka

*Department of Physics, Graduate School of Science, Kyoto University,
Kyoto 606-8502, Japan*

Recently discovered heavy fermion superconductor UTe₂ [1], as a member of the ferromagnetic superconductors [2, 3], provides a new platform to study the spin-triplet superconductivity. The spin-triplet state in UTe₂ is supported by various experimental results: large upper critical field H_{c2} along the three principal axes [1, 4], reentrant superconductivity under magnetic field along b axis [5], and the temperature dependence of the Knight shift in superconducting state [6].

In this project, we theoretically study anisotropic superconductivity in UTe₂ [7]. Theoretically, a band structure has been investigated for UTe₂ from first-principles [4]. However, previously obtained result shows insulating state with an extremely small gap, incompatible with superconducting instability. To overcome this program, we perform a GGA+ U calculation using WIEN2k package [8] and find the insulator-metal transition by Coulomb interaction. The insulator-metal transition is characterized by multi-orbital effect in Kondo lattice system. The insulator-metal transition is a peculiar property of UTe₂, which was not observed in other uranium-based superconductors nor in Kondo insulators. We can identify the three-dimensional winding number ω

and three two-dimensional \mathbb{Z}_2 numbers by Fermi surface formulas [9, 10, 11]:

$$\omega = \frac{1}{2} \sum_{K_i} n(K_i) \pmod{2}. \quad (1)$$

The GGA+ U Fermi surfaces indicate topological superconductivity for the reasonable values of U , and accompanied surface states are provided. We also predict the superconducting gap node at zero magnetic field and under magnetic field along b axis. Based on these results, we proposed multiple superconducting phases under the magnetic field.

Our another aim of this project is to study the exotic phenomena due to the spatial inversion symmetry breaking. Recently, it was found that the noncentrosymmetric Nb/V/Ta superlattice shows superconducting transition at 4.4 K [12] and exhibits nonreciprocal charge transport in superconducting state. To identify the Rashba spin-orbit interaction in the artificial superlattice [Nb/V/Ta]_n without a center of inversion, we carried out density functional theory calculations using WIEN2k package [8]. We created a slab [Nb/V/Ta]₅ containing 30 atoms, which corresponds to the five times stacking of two layers Nb, V, and Ta of a bcc structure. We obtained the Rashba splitting at the Fermi level, and the magnitude of the Rashba

splitting is around 10 meV, which originate from V atoms and is the origin of the nonreciprocity.

References

- [1] S. Ran, C. Eckberg, Q.-P. Ding, Y. Furukawa, T. Metz, S. R. Saha, I.-L. Liu, M. Zic, H. Kim, J. Paglione, and N. P. Butch, *Science* **365**, 684 (2019).
- [2] D. Aoki and J. Flouquet, *J. Phys. Soc. Jpn.* **83**, 061011 (2014).
- [3] D. Aoki, K. Ishida, and J. Flouquet, *J. Phys. Soc. Jpn.* **88**, 022001 (2019).
- [4] D. Aoki, A. Nakamura, F. Honda, D. Li, Y. Homma, Y. Shimizu, Y. J. Sato, G. Knebel, J.-P. Brison, A. Pourret, D. Braithwaite, G. Lapertot, Q. Niu, M. Vališka, H. Harima, and J. Flouquet, *J. Phys. Soc. Jpn.* **88**, 043702 (2019).
- [5] G. Knebel, W. Knafo, A. Pourret, Q. Niu, M. Vališka, D. Braithwaite, G. Lapertot, M. Nardone, A. Zitouni, S. Mishra, I. Sheikin, G. Seyfarth, J.-P. Brison, D. Aoki, and J. Flouquet, *J. Phys. Soc. Jpn.* **88**, 063707 (2019).
- [6] G. Nakamine, S. Kitagawa, K. Ishida, Y. Tokunaga, H. Sakai, S. Kambe, A. Nakamura, Y. Shimizu, Y. Homma, D. Li, F. Honda, and D. Aoki, *J. Phys. Soc. Jpn.* **88**, 113703 (2019).
- [7] J. Ishizuka, S. Sumita, A. Daido, and Y. Yanase: *Phys. Rev. Lett.* **123**, 217001 (2019).
- [8] P. Blaha, K. Schwarz, G. K. H. Madsen, D. Kvasnicka, J. Luitz, R. Laskowski, F. Tran, and L. D. Marks, *WIEN2k, An Augmented Plane Wave+Local Orbitals Program for Calculating Crystal Properties* (Karlheinz Schwarz, Techn. Universität, Wien, Austria, 2018).
- [9] M. Sato, *Phys. Rev. B* **79**, 214526 (2009).
- [10] M. Sato, *Phys. Rev. B* **81**, 220504(R) (2010).
- [11] L. Fu and E. Berg, *Phys. Rev. Lett.* **105**, 097001 (2010).
- [12] F. Ando, D. Kan, Y. Shiota, T. Moriyama, Y. Shimakawa, T. Ono *J. Magn. Soc. Japan* **43**, 17-20 (2019).

Development and applications of continuous-time quantum Monte Carlo method in the thermodynamic limit

Takahiro OHGOE

*Research Institute for Science and Engineering,
Waseda University, Okubo, Shinjuku-ku, Tokyo 169-8555*

Quantum Monte Carlo methods are powerful tools for investigating quantum many-body systems. However, they often suffer from the notorious negative-sign problem for fermionic systems and frustrated spin systems when the system-size is increased. Recently, a novel determinant quantum Monte Carlo method was proposed, which is formulated in the thermodynamic limit [1]. The method is called *connected determinant Monte Carlo method* (CDet), and its applications to the Hubbard model revealed non-trivial analytic structure of the self-energy in strongly-correlated regime [2]. Therefore, it is a promising method for tackling challenging problems of quantum many-body systems.

Here, we developed the original CDet code which is applicable to the two-component unitary Fermi gas. To show its advantage, the method was compared with the diagrammatic Monte Carlo method in the case of balanced population [3,4]. In the diagrammatic Monte Carlo method, the maximum expansion order which we could reach was 9, whereas we could

reach the 11th order in shorter CPU time by using the CDet code. Furthermore, we also obtained some results of density and Tan's contact for *imbalanced* cases where the conventional quantum Monte Carlo method suffers from the negative-sign problem. The developed code will be useful for revealing fascinating physics such as FFLO or *p*-wave superconducting instability which are expected in imbalanced populations. This work was done in collaboration with Riccardo Rossi (Flatiron institute), Felix Werner and Kris Van Houcke (ENS, Paris).

References

- [1] R. Rossi: Phys. Rev. Lett. **119** (2017) 045701
- [2] F. Simkovic IV. and E. Kozik, Phys. Rev. B **100** (2019) 121102
- [3] R. Rossi, T. Ohgoe, K. Van Houcke, and F. Werner: Phys. Rev. Lett. **121** (2018) 130405
- [4] R. Rossi, T. Ohgoe, E. Kozik, N. Prokof'ev and B. Svistunov, K. Van Houcke, and F. Werner: Phys. Rev. Lett. **121** (2018) 130406

Kitaev spin liquid under time-dependent magnetic field

Joji NASU

*Department of Physics, Yokohama National University
Hodogaya, Yokohama 240-8501*

Nonequilibrium phenomena in insulating magnets such as real-time dynamics of magnetization and transport of spin excitations have attracted considerable attention in condensed matter physics. In the insulating magnets, spin excitations are carried by magnons in the presence of a magnetic order. On the other hand, it was suggested that the spin transport can be also governed by spinons, which are elementary excitations fractionalized from spins in one-dimensional Heisenberg systems. This was confirmed in the cuprate Sr_2CuO_3 by the spin Seebeck experiments under the magnetic field.

The Kitaev quantum spin model is another candidate of the magnetic systems associated with fractional quasiparticles. In this model, the ground state is exactly shown to be a quantum spin liquid and the elementary excitations are described by two kinds of quasiparticles: itinerant and localized Majorana fermions. In this work, we study spin dynamics under the time dependent magnetic field to clarify the role of the fractional quasiparticles for the nonequilibrium phenomena.

Here, we examine the the real-time dynamics of the spin moments in the Kitaev model under the time-dependent magnetic field. In particular, we investigate the following two cases by using the Majorana mean-field theory. First, 1) we study the effect of the field quench of the uniform magnetic field to understand fundamental properties of nonequilibrium dynamics of the fractional quasiparticles in the

Kitaev model. Next, 2) we consider the effect of the time-dependent magnetic field pulse at the edge of the cluster to mimic the spin injection into the Kitaev magnet.

With respect to 1), we find that two kinds of Majorana fermions are observed separately in distinct time-scales in the time evolution of the magnetization; the low-energy localized Majorana fermions survive as long-lived excitations whereas the high-energy itinerant ones are damped in the early stage [3].

With respect to 2), we find that the propagation of the spin excitations occurs even in the absence of the magnetic field in the bulk without spin polarization. We clarified that this is attributed to the itinerant Majorana fermions [2]. We also discuss the effect of the Heisenberg interaction and extension to the $S = 1$ Kitaev model [3] on this phenomenon.

References

- [1] J. Nasu, and Y. Motome: Phys. Rev. Research **1**, 033007-1-16 (2019).
- [2] T. Minakawa, Y. Murakami, A. Koga, and J. Nasu: arXiv:1912.10599.
- [3] A. Koga, T. Minakawa, Y. Murakami, and J. Nasu: J. Phys. Soc. Jpn. **89**, 033701-1-4 (2020).

Magnetocaloric effect on the Shastry–Sutherland lattice antiferromagnet $\text{SrCu}_2(\text{BO}_3)_2$

Subaru AKIMOTO and Yasuhiro H. MATSUDA
Institute for Solid State Physics, University of Tokyo
Kashiwa-no-ha, Kashiwa, Chiba 277-8581

We have studied the magnetocaloric effect (MCE) of the Shastry–Sutherland (SS) lattice antiferromagnet $\text{SrCu}_2(\text{BO}_3)_2$ [1] with numerical simulations using the thermal pure quantum (TPQ) state. We used the $\text{H}\Phi$ as a numerical solver. The magnetic field dependence of the entropy (S_M) and specific heat (C_M) have been computed and compared with those experimentally obtained from the magnetic field variation of the MCE at different initial temperatures. Figures 1 (a) and (b) show the calculated S_M and C_M . The five trial curves and the averaged result are shown for the S_M and C_M , respectively.

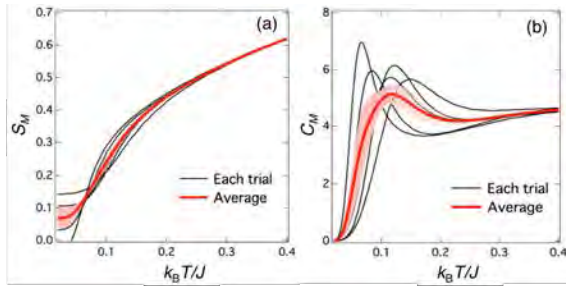


Figure 1: The five trial curves and the averaged result of the calculation with TPQ state are shown. The magnetic field is set to be 57 T corresponding to the 1/3 plateau. (a) Calculated S_M . (b) Calculated C_M .

The distinct peak is shown in the temperature dependence of the C_M at a magnetic field and the peak positions at different temperatures and magnetic fields would give the phase boundaries of the quantum spin states of the

SS lattice such as 1/4 and 1/3 plateaux [2]. The computed B – T (magnetic field – temperature) phase diagram shown in Fig. 2 is found to semiquantitatively reproduce the experimental results.

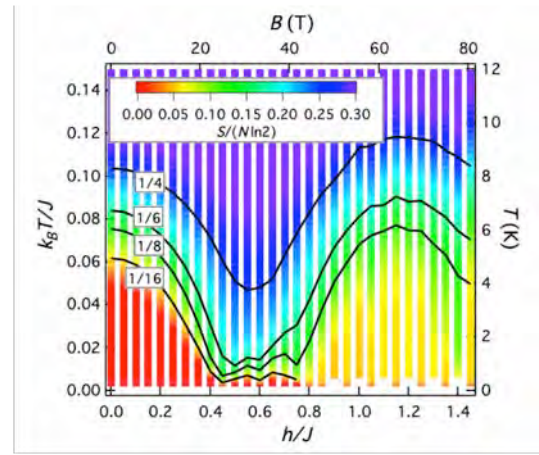


Figure 2: The calculated S_M are plotted in a B – T plane with color graduation. Several isentropic curves are also plotted.

References

- [1] H. Kageyama, K. Yoshimura, R. Stern, N. V. Mushnikov, K. Onizuka, M. Kato, K. Kosuge, C. P. Slichter, T. Goto, and Y. Ueda: *Phys. Rev. Lett.* **82** (1999) 3168.
- [2] Y. H. Matsuda, N. Abe, S. Takeyama, H. Kageyama, P. Corboz, A. Honecker, S. R. Manmana, G. R. Foltin, K. P. Schmidt, and F. Mila: *Phys. Rev. Lett.* **111** (2013) 137204.

Spin-Charge Separation in Charge Order Phase of Organic Dirac Electron System α -(BEDT-TTF) $_2$ I $_3$

Akito KOBAYASHI

*Department of Physics, Nagoya University**Nagoya 464-8602*

The organic Dirac electron system α -(BEDT-TTF) $_2$ I $_3$ exhibits a phase transition between a massless Dirac electron phase and a charge-ordered phase under pressure as shown in Fig. 1. In the charge-ordered phase, the spin gap measured by NMR, the optical gap in the optical conductivity, and the resistance gap determined by the DC resistance show completely different values and pressure dependences. The mechanism of this novel spin-charge separation has not been elucidated yet. We have theoretically studied the mechanism of the spin-charge separation in α -(BEDT-TTF) $_2$ I $_3$.

First, we have investigated the Dirac electron system with charge order in α -(BEDT-TTF) $_2$ I $_3$ using the real-space-dependent mean-field approximation, and have shown that there is a domain wall of the charge order that spontaneously appears due to ferroelectricity. We have shown that the wall-bound Dirac electrons form a one-dimensional conduction channel. Furthermore, we have shown that the linear response theory can explain the large difference between the optical gap and the resistivity gap[1].

Next, we have performed the first principles calculation for α -(BEDT-TTF) $_2$ I $_3$ under hydrostatic pressure using Quantum ESPRESSO in the Supercomputer Center, the ISSP. However, the result exhibits a type-II Dirac semimetal, which is different from the experimental results. Similar results have been independently shown by the first-principles calcula-

tions by H. Kino and T. Tsumuraya. This fact strongly suggests that the type-I Dirac electronic state observed under hydrostatic pressure cannot be explained without the strong correlation effect. We will study the type-I Dirac electronic state under hydrostatic pressure using the variational Monte Carlo method in cooperation with Dr. Yoshimi of ISSP, and then elucidate the mechanism of spin charge separation of charge-ordered phase.

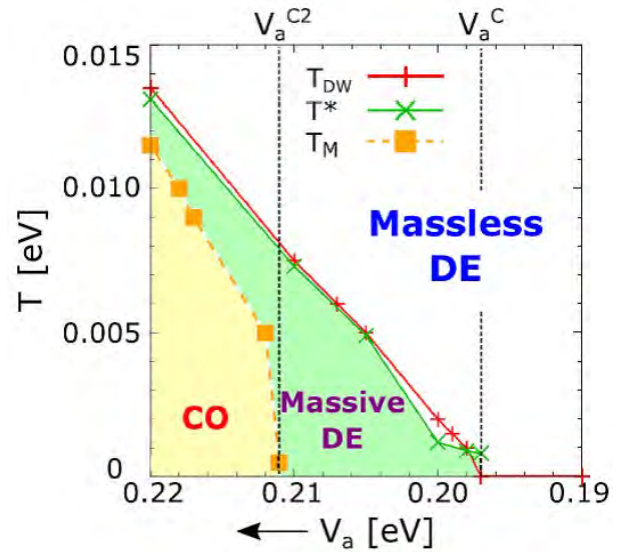


Figure 1: Phase diagram of α -(BEDT-TTF) $_2$ I $_3$.

References

- [1] D. Ohki, Y. Omori, and A. Kobayashi, *Phys. Rev. B* **100**, 075206 (2019).

Quantum Monte Carlo simulation and electronic state calculations in correlated electron systems

Takashi YANAGISAWA

Electronics and Photonics Research Institute

National Institute of Advanced Industrial Science and Technology (AIST)

AIST Central 2, 1-1-1 Umezono, Tsukuba 305-8568

Our calculations are based on the optimized variational Monte Carlo method[1, 2, 3, 4]. We have investigated the ground-state phase diagram of the two-dimensional Hubbard model and the two-dimensional d-p model. We performed parallel computation in Monte Carlo calculations. In order to reduce statistical errors, we carried out 100 ~ 200 parallel calculations. Parallel computing is very important to reduce Monte Carlo statistical errors.

We used the wave function of an $\exp(-\lambda K) - P_G$ -type wave function. This wave function is a very good many-body wave function because the ground-state energy is lowered greatly and the ground-state energy is lower than that evaluated by any other wave functions[2]. We can improve the wave function systematically by multiplying by operators P_G and $e^{-\lambda K}$ many times.

We show the phase diagram as a function of the hole doping rate x in Fig. 1. The calculations were performed on a 10×10 lattice with $U/t = 18$ and $t' = 0$. There are three phases: the antiferromagnetic insulator state (AFI), the coexistent state of antiferromagnetism and superconductivity (AF+SC) and the d -wave superconducting state (SC). Near half-filling for approximately $0 \leq x < 0.06$, the ground state is an AF insulator. The coexistent state exists for $0.06 < x < 0.09$. When the doping rate is as large as $x > 0.09$, the ground state is d -wave superconducting state. High-temperature superconductivity will occur in the SC phase in this figure.

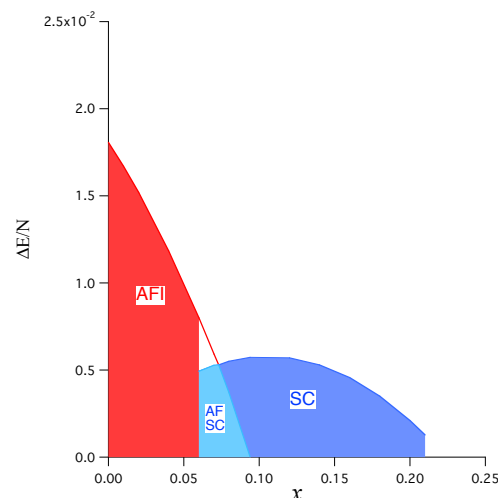


Figure 1: Phase diagram for the two-dimensional Hubbard model. The condensation energy per site as a function of the hole doping rate $x = 1 - n_e$ on a 10×10 lattice. We set $t' = 0$ and $U/t = 18$. AFI indicates the antiferromagnetic insulating state and SC denotes the d -wave SC phase. There is the coexistent state indicated as AF-S between these states.

References

- [1] T. Yanagisawa et al., J. Phys. Soc. Jpn. 67, 3867 (1998).
- [2] T. Yanagisawa, J. Phys. Soc. Jpn. 85, 114707 (2016).
- [3] T. Yanagisawa, J. Phys. Soc. Jpn. 88, 054702 (2019).
- [4] T. Yanagisawa, Condensed Matter 4, 57 (2019).

Dynamical mean-field theory + quantum Monte Carlo approach to strongly correlated electron systems with multi-orbitals

Shintaro HOSHINO

Department of Physics, Saitama University, Saitama 338-8570, Japan

The electrons with multiple orbital degrees of freedom show a variety of intriguing phenomena as realized in heavy-electron materials and also in d -electron systems such as ruthenate and iron-based superconductors. In addition, the fulleride superconductors are another example of the multiorbital electron systems [1], where the three-degenerate t_{1u} molecular orbitals are occupied by electrons originating from alkaline doping. Due to the effectively sign-inverted Hund coupling by Jahn-Teller phonons, the electrons favor the low-spin state and show superconductivity at low temperatures. Recently the experimental study has revealed the existence of anomalous metallic state near the Mott insulator [2], and the possibility of active orbital degrees of freedom is pointed out theoretically [3]. The characteristic dynamical structure in the self-energy is identified and can be a source of the anisotropic response function [4].

We have also mapped out the phase diagram of the doped fulleride, which is also experimentally realized [1]. To do this, we have analyzed the three-orbital Hubbard model with antiferromagnetic Hund's coupling by using the dynamical mean-field theory. In this theory, the many-body problem in the lattice is mapped onto the effective impurity problem without spatial periodicity, for which the continuous-time quantum Monte Carlo solver [5] has been used. Using the facilities of ISSP supercomputer, we have calculated the susceptibilities which signal the instability of the normal state toward ordering state with spontaneously broken symmetries. The exemplary

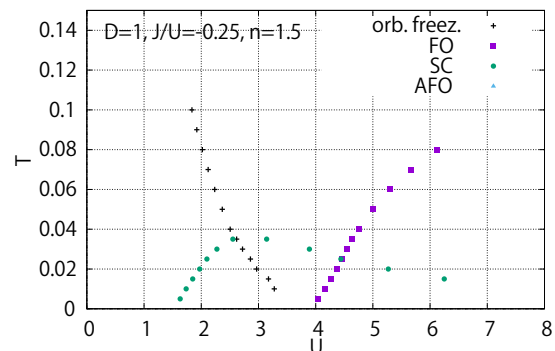


Figure 1: Temperature-interaction phase diagram. The phase boundaries for orbital ordering (FO) and superconductivity (SC) are shown, together with orbital freezing line.

results at the electron number $n = 1.5$ per molecule are shown in the figure. Here the phase diagram in the plane of temperature and Coulomb interaction is mapped out, where the horizontal axis indicates the pressure or lattice constant dependence when one compares the results with the experiments. We have demonstrated that the superconductivity appears with dome-shaped transition temperatures, while the orbital ordering dominates at large Coulomb repulsive interaction.

References

- [1] For a review, see O. Gunnarsson, *Rev. Mod. Phys.* **69**, 575 (1997). [2] R.H. Ziadik *et al.*, *Sci. Adv.* **1**, e1500059 (2015). [3] S. Hoshino and P. Werner, *Phys. Rev. Lett.* **118**, 177002 (2017). [4] S. Hoshino, P. Werner, and R. Arita, *Phys. Rev. B* **99**, 235133 (2019). [5] E. Gull *et al.*, *Rev. Mod. Phys.* **83**, 349 (2011).

Superconductivity and magnetic properties of the Hubbard model

Atsushi Yamada

*Department of Physics, Chiba University
Chiba 263-8522, Japan, Chiba 277-8581*

Frustrated magnetic systems yield a rich variety of phenomena. For example, a spin liquid state, which is a purely non-magnetic Mott insulator without spontaneously broken spatial or spin symmetry, has attracted a lot of interest. This state is realized in geometrically frustrated systems like the charge organic transfer salts κ -(BEDT-TTF)₂X[1] and Cs₂CuCl₄. [2] A simple theoretical model of these compounds is the Hubbard model on the an-isotropic triangular lattice, and spin liquid state is in fact found in this model.[3] A spin liquid could arise also in the intermediate coupling region of strongly correlated systems between a semi-metal and ordered state, because in this case a correlation-driven insulating gap might open before the system becomes ordered. This possibility might be realized in the half-filled Hubbard model on the honeycomb lattice.

We have studied the magnetic and metal-to-insulator transitions in the half-filled Hubbard model on the honeycomb lattice by variational cluster approximation using 10-site and 16-site clusters as a reference system.[5] This approach uses an exact diagonalization of the Hubbard model defined on these clusters and parts of numerical calculations were done using the computer facilities of the ISSP. Our results agree with recent large scale Quantum Monte Carlo simulations.[4] We are currently studying the effect of the frustration on various physically measurable quantities in the Hubbard model on the $\frac{1}{5}$ -depleted square lattice.

References

- [1] Y. Shimizu, K. Miyagawa, K. Kanoda, M. Maesato, and G. Saito, Phys. Rev. Lett. **91**, 107001 (2003); Y. Kurosaki, Y. Shimizu, K. Miyagawa, K. Kanoda, and G. Saito, Phys. Rev. Lett. **95**, 177001 (2005).
- [2] R. Coldea, D.A. Tennant, A.M. Tsvelik, and Z. Tylczynski, Phys. Rev. Lett. **86**, 1335 (2001); R. Coldea, D.A. Tennant, and Z. Tylczynski, Phys. Rev. Lett. **68**, 134424 (2003).
- [3] T. Yoshioka, A. Koga, and N. Kawakami, Phys. Rev. Lett. **103**, 036401 (2009); P. Sahebsara and D. Sénéchal, Phys. Rev. Lett. **100**, 136402 (2008); L.F. Tocchio, H. Feldner, F. Becca, R. Valentí, and C. Gros, Phys. Rev. B **87**, 035143 (2013); A. Yamada, Phys. Rev. B **89**, 195108 (2014); L.F. Tocchio, C. Gros, R. Valentí, F. Becca, Phys. Rev. B **89**, 235107 (2014); A. Yamada, Phys. Rev. B **90**, 235138 (2014).
- [4] S. Sorella, Y. Otsuka, and S. Yunoki, Sci. Rep. **2**, 992 (2012); F. F. Assaad and I. F. Herbut, Phys. Rev. X **3**, 031010 (2013); F. Parisen Toldin, M. Hohenadler, F. F. Assaad, and I. F. Herbut, Phys. Rev. B **91**, 165108 (2015).
- [5] A. Yamada, Int. J. Mod. Phys. B **30**, 1650158 (2016).

Exploring low-rank tensor representation of Matsubara Green's functions

Hiroshi SHINAOKA

*Department of Physics, Saitama University,
Saitama 338-8570*

We have studied a low-rank representation of two-particle Green's functions [1]. Two-particle Green's functions and the vertex functions play a critical role in theoretical frameworks for describing strongly correlated electron systems. However, numerical calculations at the two-particle level often suffer from large computation time and massive memory consumption. Example includes parquet approximation and diagrammatic non-local extensions of dynamical mean-field theory. For example, a simulation for the single-band two-dimensional Hubbard model based on the parquet approximation requires more than **a TB of memory** even at a high temperature. Thus, a compact representation of two-particle Green's functions is highly desired.

In Ref. [1], we introduced a sparse sampling scheme in the Matsubara frequency domain as well as a tensor network representation for two-particle Green's functions. The sparse sampling is based on the intermediate representation basis [2, 3, 4] and allows an accurate extraction of the generalized susceptibility from a reduced set of Matsubara frequencies. The tensor network representation provides a system independent way to compress the information carried by two-particle Green's functions.

We used System B at the ISSP supercomputer center to demonstrate efficiency of the present scheme for calculations of static and dynamic susceptibilities in single- and two-band Hubbard models in the framework of dynamical mean-field theory.

Figure 1 shows the dynamical lattice susceptibility computed by Bethe-Salpeter equation (BSE) based on dynamical mean-field theory for a two-band Hubbard model. In solving BSE, we compressed the local two-particle Green's function using the tensor-network representation. The uncompressed data takes up **700 MB** even on the sparse grid, while the tensor network representation takes up only **330 kB** for $D = 60$. Here, D is a bond dimension in the tensor network.

In future studies, we will use the new techniques to study real compounds by means of the non-local extension of the dynamical mean-field theory and the parquet approximation.

This report is based on the collaboration with D. Geffroy, M. Wallerberger, J. Otsuki, K. Yoshimi, E. Gull, J. Kuneš.

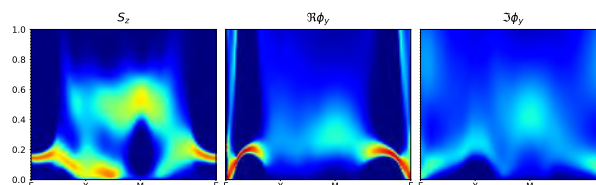


Figure 1: Dynamical lattice susceptibility computed for a two-band Hubbard model. Reproduced from Ref. [1] under the CC BY 4.0 license.

References

- [1] H. Shinaoka, D. Geffroy, M. Wallerberger, J. Otsuki, K. Yoshimi, E. Gull, J. Kuneš,

SciPost Phys. **8**, 012 (2020)

- [2] H. Shinaoka, J. Otsuki, M. Ohzeki and K. Yoshimi, Phys. Rev. B **96**, 035147 (2017)
- [3] H. Shinaoka, J. Otsuki, K. Haule, M. Wallerberger, E. Gull, K. Yoshimi and M. Ohzeki, Phys. Rev. B **97**, 205111 (2018)
- [4] J. Otsuki, M. Ohzeki, H. Shinaoka and K. Yoshimi, Sparse modeling in quantum many- body problems, J. Phys. Soc. Jpn. **89**, 012001 (2020)

Photoinduced dynamics and high harmonic generation in magnetism

Sumio Ishihara

Department of Physics, Tohoku University

Sendai 980-8578

Nonequilibrium susceptibility in Floquet states

Recent great progress in laser light technology significantly promotes scientific research in strongly coupled light-matter systems. One of the fascinating phenomena induced by the strong light-matter coupling is the appearance of the Floquet states, in which a time-periodic electromagnetic field behaves as photons and hybridizes with electrons. We examine the spin/charge susceptibility in photoinduced Floquet states [1]. We consider a free-electron system coupled to a fermionic heat bath. We adopt the Hamiltonian given by

$$H = \sum_{ks} \varepsilon_k c_{ks}^\dagger c_{ks} + \sum_{\nu} b_{\nu}^\dagger b_{\nu} + \sum_{ks\nu} V_n u \left(c_{ks}^\dagger b_{\nu} + b_{\nu}^\dagger c_{ks} \right), \quad (1)$$

where c_{ks}^\dagger is a creation operator of an electron with momentum k and spin $s(=\uparrow, \downarrow)$, and b_{ν}^\dagger is that of a fermion in a bath with a quantum number ν .

The susceptibility is formulated on the basis of the Floquet Green's function method, and its perturbative expression is derived from a series expansion. Through the numerical calculations, we have the following results.

1) In the case of the large electric-field frequency Ω in comparison with the electron bandwidth, we demonstrate that the bandwidth reduction due to the dynamical localization effect enhances the susceptibility and a deformation of the Fermi surface which depends on light polarization shifts the peak positions of the susceptibility (Fig. 1).

2) On the other hand, in the case of small Ω comparable to the bandwidth, the multiple Floquet bands cross the Fermi level of the bath and the additional peaks emerge at momenta corresponding to “nesting vectors” between the Floquet-band Fermi surfaces (Fig. 2).

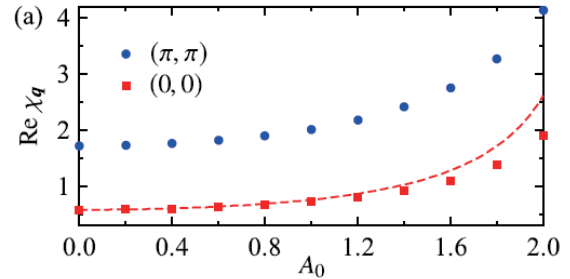


Figure 1: The susceptibility at $q = (0, 0)$ and (π, π) as a function of the light amplitude A_0 [1].

Optical response in the excitonic insulating state

The excitonic insulating (EI) state was proposed more than a half century ago in semiconductors and semimetals and has been studied intensively on both the experimental and theoretical sides. We study the optical responses in EI states [2]. We adopt the two-orbital Hubbard model with finite energy difference between the orbitals defined by

$$H = \Delta \sum_{i\sigma} (n_{ia\sigma} - n_{ib\sigma}) + \sum_{\langle ij \rangle \alpha \sigma} t_{\alpha} c_{i\alpha\sigma}^\dagger c_{j\alpha\sigma} + \sum_i (U \sum_{\alpha} n_{i\alpha\uparrow} n_{i\alpha\downarrow} + U' n_{ia} n_{ib})$$

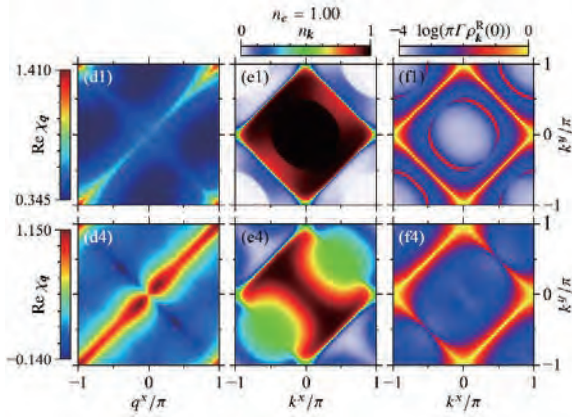


Figure 2: The susceptibility, the momentum distribution function; and the spectral function at $\omega = 0$, under the linearly polarized light of $A_0 = 0.4$ and 1.6 [1].

$$\begin{aligned}
 & + J \sum_{i\sigma\sigma'} c_{i\alpha\sigma}^\dagger c_{i\beta\sigma'}^\dagger c_{i\alpha\sigma'} c_{i\beta\sigma} \\
 & + I \sum_{i\alpha} c_{i\alpha\uparrow}^\dagger c_{i\alpha\downarrow}^\dagger c_{i\alpha\downarrow} c_{i\alpha\uparrow}, \quad (2)
 \end{aligned}$$

where $c_{i\alpha\sigma}$ is an annihilation operator of an electron with spin $\sigma (= \uparrow, \downarrow)$ and the orbital $\alpha (= a, b)$ at site i , and $n_{i\alpha\sigma} = c_{i\alpha\sigma}^\dagger c_{i\alpha\sigma}$ is the particle number operator.

The variational cluster approach method was applied to the two-orbital Hubbard model with a finite energy difference between the orbitals. In the analyses of the ground state, we considered possibilities of the low-spin state, the high-spin antiferromagnetic state, the EI state. The optical conductivity spectra were formulated by the Green's function method, where the vertex correction is taken into account. Figure 3 shows the optical conductivity spectra. In the EI phase, a new peak around $\omega/t \sim 10$ and a continuum around $3 < \omega/t < 8$ appear. The intensity of the EI component increases with increasing J/t in the EI phase. It is shown that the intensity of this structure at low temperatures almost follows the EI order parameter.

These researches have been performed with collaboration with A. Ono, H. Li, M. Naka and J. Ohtsuki. The numerical calculations in

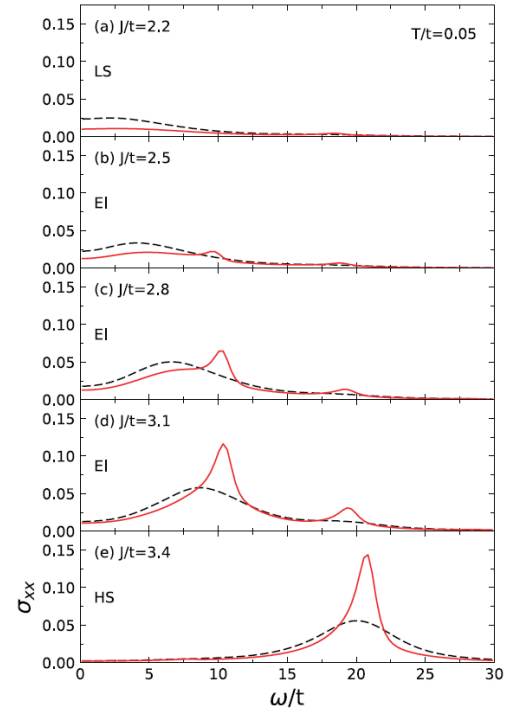


Figure 3: Optical conductivity spectra for several values of the Hund coupling J . The red solid lines show results including the vertex corrections, while the black dashed results show results without the vertex corrections. [2].

these works have been done using the facilities of the Supercomputer Center, the Institute for Solid State Physics, the University of Tokyo.

References

- [1] A. Ono and S. Ishihara: Phys. Rev. B **100**, 075127 (2019).
- [2] H. Li, J. Otsuki, M. Naka and S. Ishihara Phys. Rev. B **101** 125117 (2020).

Mechanism of superconductivity and electron-hole asymmetry in molecular conductors

κ -(BEDT-TTF)₂X

Hiroshi WATANABE

Cluster for Pioneering Research (CPR), RIKEN

2-1 Hirosawa, Wako-shi, Saitama 351-0198

The family of quasi two-dimensional molecular conductors κ -(BEDT-TTF)₂X has been extensively studied as a typical example of strongly correlated electron system. Depending on the monovalent anion X, they show various quantum phases such as antiferromagnetic (AF) and spin-liquid dimer-Mott insulators, and superconductivity (SC) [1]. Owing to the similarities in the experimental phase diagrams, κ -(BEDT-TTF)₂X system is often compared with high- T_c cuprates, which exhibit Mott metal-insulator transition and SC [2]. Recently, carrier doping in κ -(BEDT-TTF)₂X has been realized using electric-double-layer transistor [3], and the direct comparison with cuprates becomes possible. The experimental result shows the electron-hole doping asymmetry, reminiscent of the high- T_c cuprates.

Here, we theoretically study the doping effect in κ -(BEDT-TTF)₂X. We consider a four-band extended Hubbard model including on-site (U) and intersite Coulomb interactions (V_{ij}) with κ -type geometry with the largest hopping integral t_{b1} as an energy unit. The ground state properties are studied with the variational Monte Carlo (VMC) method. The Gutzwiller-Jastrow type wave function is used for the VMC trial wave function. The system sizes for calculation are from 288 ($2 \times 12 \times 12$) to 1152 ($2 \times 24 \times 24$).

Figure 1 shows the ground-state phase diagram of the extended Hubbard model for κ -(BEDT-TTF)₂X [4]. We find significant

electron-hole doping asymmetry in the phase diagram where AF spin order, different patterns of charge order, and SC compete with each other. Hole-doping stabilizes the dimer-type AF phase and promotes SC with d_{xy} -wave symmetry, which has similarities with high- T_c cuprates. In contrast, in the electron-doped side, geometrical frustration destabilizes the AF phase and the enhanced charge correlation induces another SC with extended- $s+d_{x^2-y^2}$ -wave symmetry. Our results disclose the mechanism of each phase appearing in filling-control molecular Mott systems, and elucidate how physics of different strongly-correlated electrons are connected, namely, molecular conductors and high- T_c cuprates.

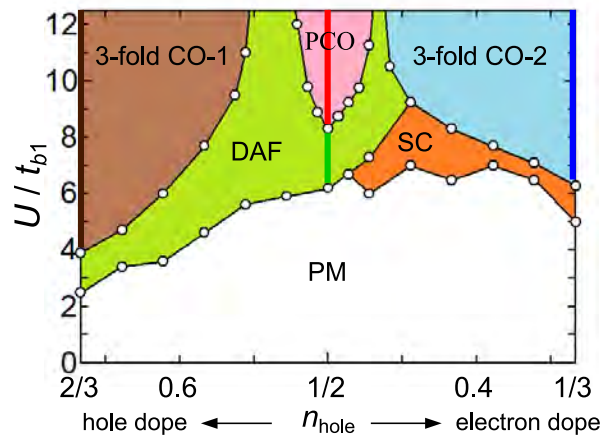


Figure 1: Ground-state phase diagram of the extended Hubbard model for κ -(BEDT-TTF)₂X [4].

References

- [1] K. Kanoda: J. Phys. Soc. Jpn. **75** (2006) 051007.
- [2] R. H. McKenzie: Science **278** (1997) 820.
- [3] Y. Kawasugi et al., Sci. Adv. **5** (2019) eaav7282.
- [4] H. Watanabe, H. Seo, and S. Yunoki: Nat. Commun. **10** (2019) 3167.